JOURNAL OF PETROLOGY | VOLUME 39 | NUMBER 2 | PAGES 191–225 | 1998

Etendeka Volcanism of the Goboboseb Mountains and Messum Igneous Complex, Namibia. Part I: Geochemical Evidence of Early Cretaceous Tristan Plume Melts and the Rọle of Crustal Contamination in the Parana–Etendeka CFB

A. EWART[1]*, S. C. MILNER[2]†, R. A. ARMSTRONG[2]‡ AND A. R. DUNCAN[2]

[1]DEPT. OF EARTH SCIENCES, UNIVERSITY OF QUEENSLAND, ST. LUCIA, QLD. 4072, AUSTRALIA

[2]DEPT. OF GEOLOGICAL SCIENCES, UNIVERSITY OF CAPE TOWN, RONDEBOSCH 7700, SOUTH AFRICA

RECEIVED FEBRUARY 23, 1996; REVISED TYPESCRIPT ACCEPTED JULY 30, 1997

The Goboboseb Mountains and Messum Complex represent a major Cretaceous (132 Ma) bimodal eruptive centre in the southern Etendeka continental flood basalt (CFB) province. The eruptives comprise the Awahab Formation and are represented by a lower sequence of mafic lavas, followed by the Goboboseb quartz latite members, the Messum Mountain Basalts, and finally the Springbok quartz latite. The sequence is cut by numerous dolerite dykes, sills and plugs, rare rhyolite, and carbonatite. The mafic lavas comprise two distinct series, which although corresponding broadly to the Etendeka regional low Ti and Zr basalts (LTZ type), are distinguished by Ti/Zr ratios into the LTZ.H (higher Ti/Zr) and LTZ.L (lower Ti/Zr) series. The LTZ.H basalts have no previously described extrusive equivalent in the Etendeka (or Parana) CFB, and consist of magnesian, mildly alkaline to tholeiitic lavas, dominated by oliv + cpx phenocryst assemblages which fractionate (near the surface) to phono-tephrite. They are identified as predominantly mantle plume melts (Tristan–Walvis plume). The LTZ.L lavas are less magnesian, extending to icelandites, are tholeiitic, with cpx ± oliv + pl + Fe–Ti oxide phenocryst assemblages, and groundmass pigeonite and subcalcic augite. Stratigraphically, the LTZ.H lavas are interbedded with LTZ.L types in the lower part of the sequence and also occur as dykes. Within the Messum Complex, a remnant early sequence of basalts (Messum Crater Basalts) are in part transitional between the LTZ.L and LTZ.H series. The LTZ.H, and at least some of the LTZ.L lavas are inferred to have been erupted from the Goboboseb–Messum Centre. Chemically, the LTZ.H melts are broadly intermediate between E-MORB and OIB magmas, with higher Ti/Zr, Sm/Yb and Ti/Y ratios than the LTZ.L types, which suggest segregation depths between the garnet and spinel peridotite stability fields. The Pb–Nd–Sr isotopic compositions of the LTZ.H eruptives are similar to, but not identical with the modern Tristan plume composition, and the observed variability is attributable to limited lower-crust assimilation and/or Atlantic MORB source mixing. The LTZ.L lavas show evidence for crystal fractionation, have 'arc-like' trace element signatures, correlated ε_{Sr}–SiO_2, ε_{Sr}–Ti/Y and –Ti/Zr, ε_{Sr}–1/Sr and 1/Nd–ε_{Nd} variations, and relatively radiogenic Pb, evolved Sr(ε_{Sr} 58–174) and low Nd(ε_{Nd} –6·1 to –9·5) isotopic compositions. Their geochemistry is inferred to be AFC (assimilation–fractional crystallization) controlled, and is modelled by three-component mixing involving mantle plume derived melt, mafic lower crust and silicic mid–upper crust. The voluminous quartz latites (Part II, Ewart et al., 1978) extend these geochemical trends.

KEY WORDS: *Etendeka–Parana volcanism; plume magmas; crustal contamination; three-component mixing; lower crust*

*Corresponding author. e-mail: tonye@earthsciences.uq.edu.au

† Present address: Geological Survey, Ministry of Mines and Energy, P.O. Box 2168, Windhoek 9000, Republic of Namibia.

‡ Present address: Research School of Earth Sciences, The Australian National University, Canberra, A.C.T. 0200, Australia.

INTRODUCTION

The Etendeka Group volcanic rocks of the Goboboseb Mountains and the Messum Igneous Complex are a southeasterly remnant of the combined Parana (Brazil)–Etendeka (Namibia) continental flood basalt (CFB) Province. Volcanic rocks in the Parana–Etendeka Province have an estimated volume in excess of 800 000 km^3 (Peate & Hawkesworth, 1996). Although the Etendeka represents a relatively small proportion of this volume (<10%), the excellent rock exposure in the Namib Desert environment makes it a crucial area for both the understanding of the detailed stratigraphy (at least in the eastern part of the province) and the recognition of potential eruptive centres. In the Parana, recent dating constrains the age of magmatism to the interval 127–138 Ma (Baksi *et al.*, 1991; Hawkesworth *et al.*, 1992; Renne *et al.*, 1992; Turner *et al.*, 1994; Stewart *et al.*, 1996), although Renne *et al.* (1996*a*) reported an age range of 129–131 Ma for the Ponta Grassa dyke swarm. The most recent Ar–Ar dating of southern Etendeka volcanic rocks and associated intrusions suggests an age range of 129–132 Ma (Renne *et al.*, 1996*b*) and 127–130 Ma (Stewart *et al.*, 1996).

Although the Parana–Etendeka Province is commonly referred to as a continental flood basalt province, the volcanic association is strictly bimodal, with significant volumes of rhyolite (*sensu lato*) which is spatially and temporally linked with numerous subvolcanic intrusions in both Namibia and Brazil. This paper (Part I) focuses on the petrology and geochemistry of the mafic lavas. A companion paper (Part II, Ewart *et al.*, 1998) discusses the associated suite of very large volume silicic eruptive units occurring within the Goboboseb Mountains. The eruptive centre of the silicic units and at least some of the mafic lavas is inferred to be the Messum Igneous Complex (Korn & Martin, 1954; Milner & Ewart, 1989).

Magmatism of the Parana–Etendeka Province is clearly related in space and time to a combination of mantle plume upwelling and continental rifting, and is linked to the Tristan da Cunha hotspot via the Rio Grande Rise and Walvis Ridge (e.g. O'Connor & Duncan, 1990; Peate *et al.*, 1990; Hawkesworth *et al.*, 1992). Despite this apparent link, and as emphasized by Peate & Hawkesworth (1996), no picritic basalts or basalts with an appropriate plume-type geochemical component have been reported in the Parana–Etendeka Province. In this paper we document the occurrence of two basaltic lava series. Although both chemically correspond broadly to the Etendeka regional low Ti and Zr basalts (LTZ types; also referred to as the Tafelberg magma type; Erlank *et al.*, 1984), in the Goboboseb Mountains region we can readily distinguish the two series on the basis of Ti/Zr ratios. We have designated the series with higher Ti/Zr ratios as the LTZ.H series [the Tafelkop magma type noted by Milner & le Roex (1996)], and those with lower Ti/Zr ratios as the LTZ.L series (in fact, as shown below, similar to the regional LTZ types). The LTZ.H series are magnesian and mildly alkaline to tholeiitic lavas, which are interpreted here as being plume derived. In addition, we investigate the role of crustal contamination of these plume-derived melts to account for the compositional characteristics of the more abundant low Ti–Zr (LTZ and LTZ.L) basalts of the Parana–Etendeka Province.

THE GOBOBOSEB MOUNTAINS AND MESSUM IGNEOUS COMPLEX

Geological setting

The pre-volcanic basement comprises Proterozoic (1·7–2·1 Ga) metamorphic rocks marking the southern margin of the Congo Craton; this is bounded laterally to the west and southeast, and locally overlain by wide belts of mixed sedimentary and volcanic rocks of the Pan-African (470–930 Ma) Damara sequence (Miller, 1983; Henry *et al.*, 1990). The basement is overlain by discontinuous Mesozoic Karoo sedimentary sequences throughout the southern portion of the Etendeka, which in turn underlie the Etendeka Group.

The Etendeka Group consists of a bimodal association of mafic to intermediate (51–59% SiO_2), predominantly tholeiitic, lavas interbedded with more silicic (66–69% SiO_2) quartz latite units. Outcrop remnants of these volcanic rocks are preserved along the northwestern Namibian coast and adjacent inland areas (Fig. 1), and are associated with abundant dolerite dykes and a series of subvolcanic intrusive complexes (Erlank *et al.*, 1984; Milner *et al.*, 1995*c*). The latter lie along a broad northeasterly trending zone, extending inland from Cape Cross (Fig. 1) for ~350 km. Details of their distribution have been given by Martin *et al.* (1960), who divided them into granitic complexes (e.g. Brandberg), differentiated mafic complexes (e.g. Messum, Cape Cross), and alkaline and carbonatitic complexes (e.g. Paresis). Those workers interpreted some of these complexes, including Messum, as caldera collapse structures.

The Goboboseb sequence

In the southern Etendeka, the volcanic sequence comprises the Awahab and Tafelberg Formations (Milner *et al.*, 1995*a*). Although the outcrop patterns of both Formations are juxtaposed, the Awahab Formation is distributed over the southernmost part of the Etendeka and throughout the Goboboseb Mountains (Fig. 2). The Goboboseb Mountains form an asymmetrical apron around the Messum Igneous Complex (Messum 'Crater'; Fig. 2), the latter being interpreted as the major eruptive

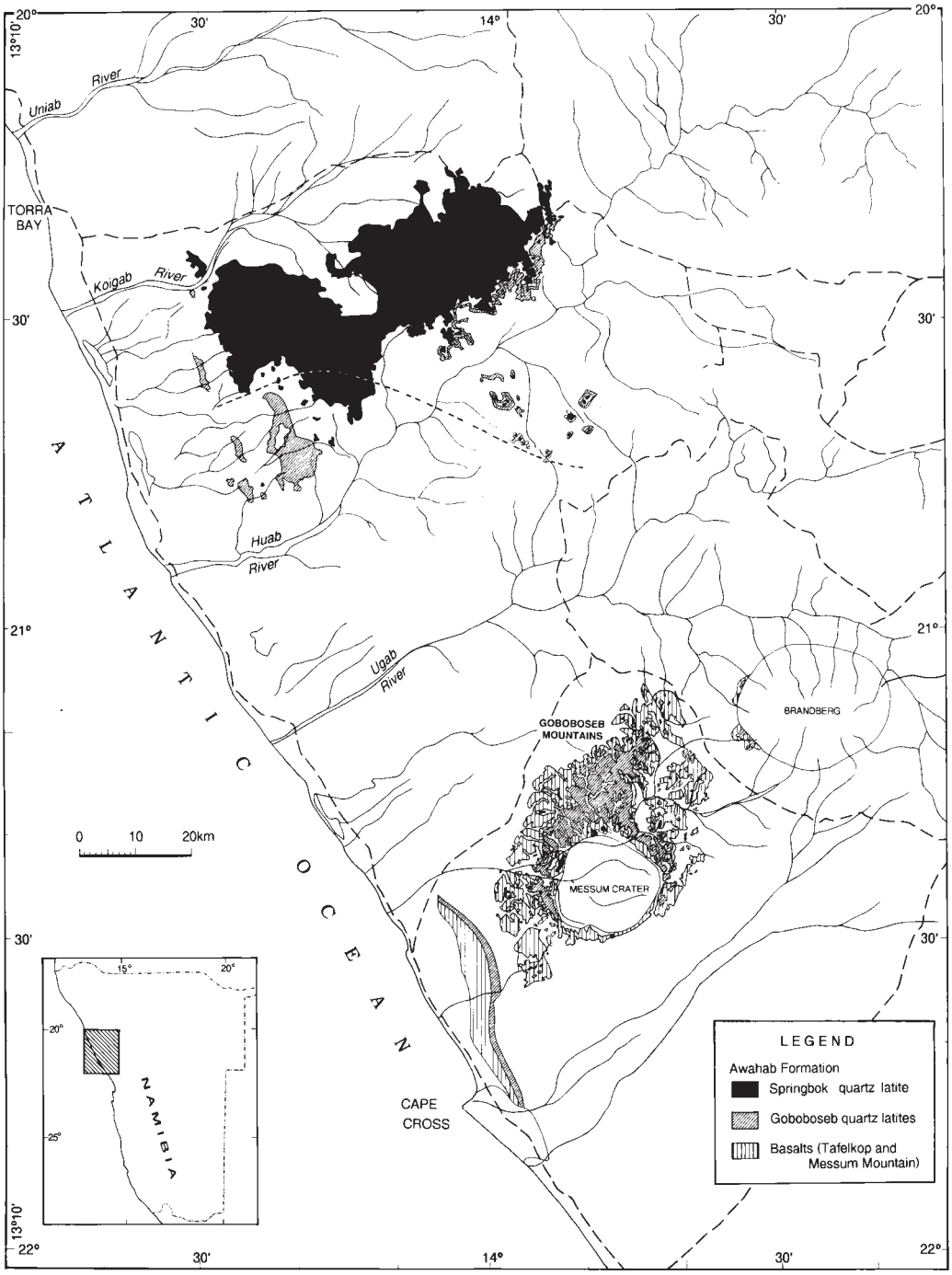

Fig. 1. Map of Southern Etendeka and Messum showing distribution of the Awahab silicic and mafic (southern area only) eruptives. The short-dashed line represents approximate southern limit of the occurrences of phenocrystal hypersthene in the Springbok quartz latite. Heavier longer-dashed lines represent major roads.

centre for the Awahab silicic units (Milner *et al.*, 1995*b*). The rock sequences within the Goboboseb lie within a regional sag structure believed to result from massive magma withdrawal during quartz latite eruptions (Milner & Ewart, 1989).

In the Goboboseb Mountains the Awahab Formation (Table 1) comprises interbedded basalts and quartz latites (QL) with an estimated minimum thickness of 600 m, which lie unconformably on Damara basement and Karoo sandstones. The lower 250 m of the sequence, the Tafelkop Basalt Member, consists of multiple basalt flows with individual thicknesses of 5–30 m. The lower portion of the Tafelkop Member is dominated by simple flow units which give way to more altered compound flows higher in the sequence. These basalts are overlain by three quartz latite flow units (QL Units I, II and III) which together constitute the Goboboseb Quartz Latite Member, with a thickness of 100–150 m. A prominent basalt flow, the Copper Valley Basalt, fills a north–south trending palaeovalley extending northwards from Messum and lies stratigraphically between QL Units I and II. This flow has an observed maximum thickness of 170 m and is a petrographically and chemically distinctive icelandite. Other, more localized, basaltic flows are intercalated between Goboboseb QL Units I and III to the northeast and west of Messum. The Goboboseb Quartz Latite Member is in turn overlain by the Messum Mountain Basalt (MMB) Member, which comprises 130 m of basalt flows preserved as relatively narrow outcrops around the northern and western margin of Messum. A fourth quartz latite, the Springbok Quartz Latite Member, forms the uppermost part of the Goboboseb sequence.

The Goboboseb volcanic units are cut by numerous dolerite dykes and sills, four gabbroic plugs, and rare rhyolite and carbonatite dykes. Of particular significance is the occurrence of quartz monzonite intrusions, chemically and mineralogically equivalent to both the Goboboseb and Springbok quartz latite units. These occur as two plug-like bodies intruding the Goboboseb Quartz Latite Member just north of the northern Messum rim, and as a composite laccolith (up to 30 m thick) intruding between the base of the volcanic succession and the underlying Karoo sandstones around the southern edge of Messum.

The source of the Goboboseb and Springbok quartz latites is thus specifically linked to the Messum Complex and its immediate vicinity (Milner & Ewart, 1989). In addition to the Goboboseb Mountains, these quartz latite units are distributed over large parts of the southern Etendeka and southeastern Parana (Milner *et al.*, 1992, 1995*b*) and are the erupted products of a massive (>8000 km^3) silicic magma system which we term the Awahab magma system. The source of the Goboboseb basalts is less clear, the alternatives being either eruption from Messum and the immediately surrounding region, or eruption as part of the regional Etendeka flood basalt lavas from the regional dolerite dyke swarms. The abundant dolerite dykes, sills and plugs in the Goboboseb Mountains, including the occurrence of certain chemically distinctive dykes and lavas (described below) within the Tafelkop Member, suggest that at least some of the basalts emanated from a volcanic edifice associated with Messum, and have been preserved as a result of the regional sag structure. The distributions of the MMB, the Copper Valley Basalt and other intercalated basalt flows between the quartz latite units indicate that they erupted from Messum.

The Messum Igneous Complex

The Messum Complex is roughly circular in plan and ~18 km in diameter. The structure is well defined topographically, although contacts with the surrounding Goboboseb volcanic rocks are largely obscured by sand except along the eastern and southeastern margins, where near-vertical, sheared quartz latites and basalts are exposed at the contact. Quartz latite and basalt outcrops peripheral to the complex exhibit contact metamorphism, which is most intense along the eastern and southern margins.

The evolutionary history of the Messum Complex is difficult to decipher owing to the nature of the outcrop and the diversity of intrusive and extrusive rock types. The latter form one of the earliest phases of the Messum Complex. Two major arcuate ridges of basalt outcrop occur within the eastern to northeastern and southern outer segments of the complex (Fig. 2). Termed the Messum Crater Basalts (MCB), these basalts comprise clinopyroxene-phyric, plagioclase-phyric, aphyric and amygdaloidal varieties. They are locally sheared, and are extensively intruded by dykes, veins and larger irregular bodies of xenolithic granitoids (containing MCB xenoliths) and xenolith-free aplitic granite. The incomplete arcuate outcrop pattern, together with their structure, suggests that the MCB represent an early subsidence phase of Messum. Problematically, the MCB cannot be unambiguously correlated chemically or petrographically with the Tafelkop basalts, although it is expected that they should correlate stratigraphically with the lower part of the sequence; this may reflect in part the extent of granitic intrusion and recrystallization, although the MCB do contain some pyroxene-phyric types, not recognized in the Goboboseb sequence.

Volcanic breccias and lava domes form the central hills of the Messum Complex, the Messum Core. A predominance of monomict rhyolite breccias leaves little doubt that a significant rhyolitic centre existed in what is now the northeastern part of the Messum Core. This

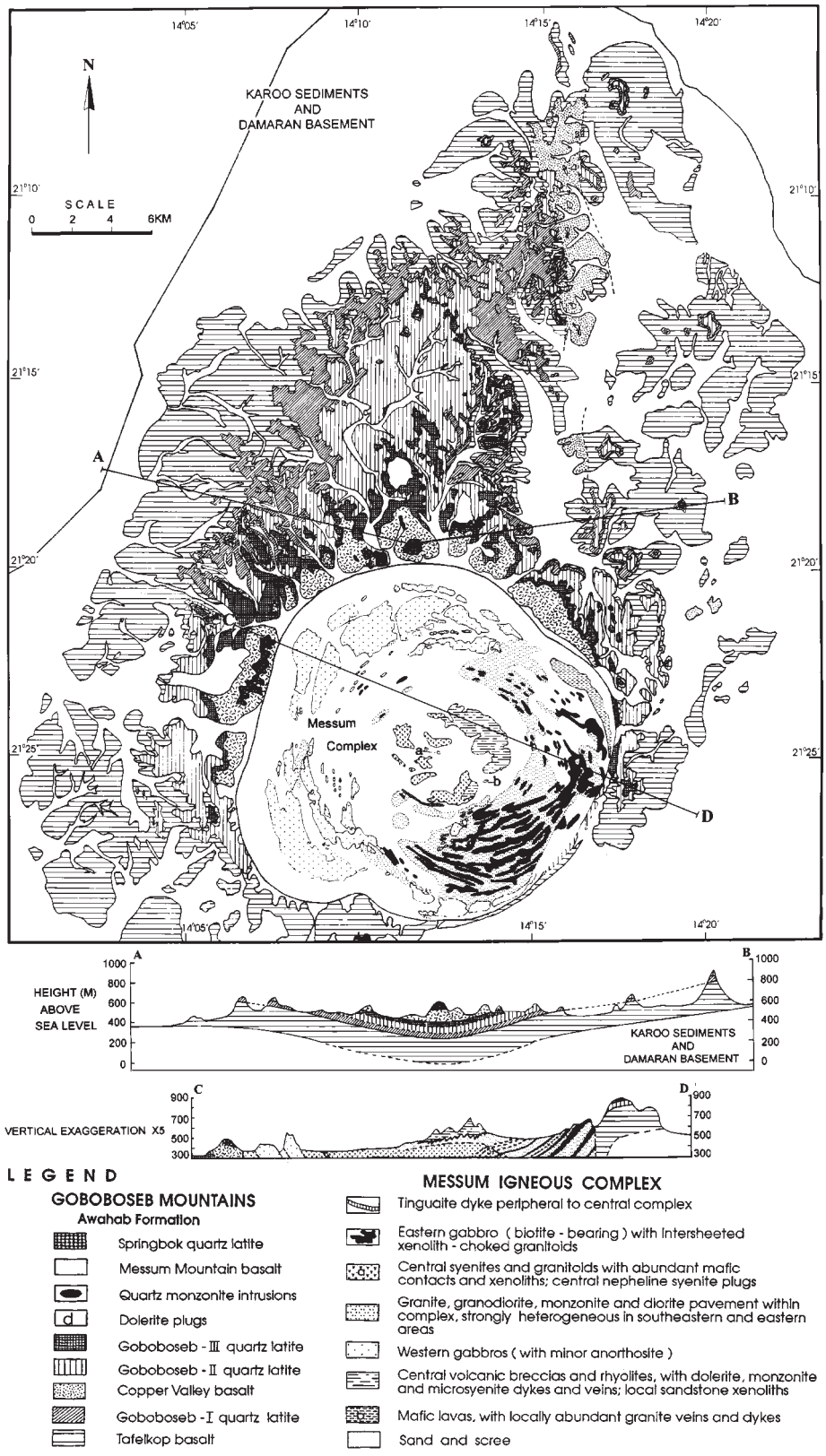

Fig. 2. Geological map of the Goboboseb Mountains and Messum. Modified from Milner & Ewart (1989) and Korn & Martin (1954), respectively. Heavy dark lines represent roads.

Table 1: Stratigraphy and nomenclature of volcanic members within Awahab Formation

Member	Thickness in Goboboseb Mts (m)	Abbreviation used
Springbok Quartz Latite	>70	Springbok QL
Messum Mountain Basalt	130	MMB
Goboboseb Quartz Latite		
Goboboseb—III quartz latite*	10–20	Goboboseb QL III
Goboboseb—II quartz latite*	50–>90	Goboboseb QL II
Copper Valley basalt*—(valley infilling)	130	Copper Valley icelandite
Goboboseb—I quartz latite*	30–>70	Goboboseb QL I
Tafelkop Basalt	250–300	

* Informal name. After Milner *et al.* (1995*a*).

rhyolite centre is extensively hornfelsed and intruded by dykes and sheets of micro-syenite, dolerite and granite. Large quartzite bodies (up to 1 km strike length) interbedded with the rhyolites are interpreted as recrystallized sandstone bodies, probably equivalent to the Karoo sandstones underlying the Goboboseb sequence. Basaltic clasts in the breccias also contain quartzite and Damara basement xenoliths. The presence of these exotic lithologies, together with interbedded sandstones and the extensive hornfels alteration, supports the interpretation that the volcanic phases forming the Messum Core represent the earliest, uplifted sequence in the history of Messum. As will be shown, the volcanic lithologies represented in the breccias are geochemically distinct from the Goboboseb volcanic sequences.

The oldest intrusions in Messum are best exposed in the eastern and southern parts of the complex, although isolated outcrops in the largely sand covered 'moat' region, between the core and the peripheral margin in the northern and western areas, indicate a much larger extent. These intrusions consist of sheets and more irregular-shaped bodies with lithologies including mafic diorite, monzonite, quartz syenite, heterogeneous granite and granite with abundant (up to 60% by volume) mafic inclusions. The relationships between the different intrusive phases is complicated and provides evidence of extensive magma mingling, and available chemical and petrographic data suggest that more thorough magma mixing occurred between the 'moat' granitoids and the quartz syenite–granite phases of the outer core. The next major intrusive phases in Messum are gabbroic. Two distinct gabbroic cone sheet centres are recognized, the eastern gabbroic centre (eastern gabbros) which consists dominantly of biotite-bearing olivine gabbronorites and is inferred to be the older of the two gabbroic centres. The western centre (western gabbros) consists of cumulate anorthosite, troctolite, olivine gabbro and gabbro, cut by dykes and sills of microgabbro. The last major intrusions in Messum are of nepheline syenite, intruding the inner core region of the complex.

From the viewpoint of this paper, it is noted that Messum shows evidence for the simultaneous existence of mafic and silicic magmas and a close temporal relationship between the eastern gabbros and the 'moat' intrusions. Magma mingling is inferred to have produced the heterogeneous granitoids. The western gabbros sharply intrude the heterogeneous granite–diorite association, and by implication postdate the eastern gabbros.

Volcanic and intrusive age relationships

Milner *et al.* (1995*c*) reported Rb–Sr internal isochron ages of 132 ± 2·2 Ma (Messum eastern gabbro), 129·8 ± 3·8 Ma (Goboboseb QL I) and 126·8 ± 1·3 Ma (nepheline syenite from Messum Core). These workers suggested that the main Etendeka volcanism occurred between 132 and 135 Ma, with magmatism in the various regional central complexes ranging between 124 and 137 Ma. Renne *et al.* (1996*b*) reported ages, based on the more precise ^{39}Ar–^{40}Ar technique, of 131·7 ± 0·7 Ma (quartz diorite, eastern moat), 132·1 ± 0·7 Ma (eastern gabbro), 132·1 ± 1·2 Ma (anorthosite, western gabbros), 129·3 ± 0·7 Ma (nepheline syenite, Messum Core), 132·1 ± 0·4 Ma (Goboboseb QL I), 131·90 ± 0·5 Ma (Goboboseb QL II) and 132·0 ± 0·7 Ma (Springbok QL). These dates indicate that the emplacement of the Messum intrusions (except the central nepheline syenite plugs) and the eruption of the Goboboseb and Springbok quartz latites overlap within experimental error, at 132 Ma. Stewart *et al.* (1996) reported two ^{39}Ar–^{40}Ar dates of 127 and 129 Ma, for hornblende and biotite from Messum gabbros.

The Messum intrusions cut and metamorphose the Goboboseb Mountains volcanic sequence, with the latest movement along the eastern side of the Messum ring fault postdating the Springbok QL eruption. K–Ar dates on the Brandberg complex of 125–135·5 Ma (Watkins *et al.*, 1994) are therefore inconsistent with the previous data, notably the older ages reported for granites which in fact intrude and truncate both the Tafelkop and Goboboseb Members.

ANALYTICAL METHODS

Major and trace elements

After initial splitting and jaw crushing, samples were pulverized in a carbon-steel swing mill for constant time. Major and trace elements were determined by X-ray fluorescence (XRF) at the University of Cape Town, using the procedures of Norrish & Hutton (1969). H_2O^- and loss on ignition were determined at 110°C and 850°C (12 h), respectively. Na_2O and trace elements were analysed on pressed powder briquettes, whereas other major elements were determined on fused glass discs.

A subset of samples were analysed by instrumental neutron activation analysis at the Australian National University (Dr B. W. Chappell), following the procedures of Chappell & Hergt (1989).

Microprobe analyses were carried out on a Cameca Camebax Electron Microprobe at the University of Cape Town, using pure mineral samples as standards, and ZAF and Bence & Albee (1968) correction procedures.

Isotopic compositions

All isotope ratios were measured on a VG-Sector seven-collector mass spectrometer at the Radiogenic Isotope Facility, Department of Geological Sciences, University of Cape Town, using unleached sample powders. Sr isotopes were measured in dynamic mode using the mass fractionation correction $^{86}Sr/^{88}Sr = 0{\cdot}1194$, and the $^{87}Sr/^{86}Sr$ ratios reported are normalized to the NBS SRM987 value of 0·71022. Nd isotopes were also measured in dynamic mode, are corrected for mass fractionation using $^{146}Nd/^{144}Nd = 0{\cdot}7219$, and are normalized to the present-day $^{143}Nd/^{144}Nd$ value of 0·51264 for BCR-1, which is equivalent to $^{143}Nd/^{144}Nd = 0{\cdot}51184$ for the La Jolla standard. Pb isotope analyses were measured in static mode and frequent measurement of NBS SRM981 provided estimates for mass fractionation, which was within 0·08–0·10%/a.m.u. Within-run precision on individual ratio measurements is given by the ($2\sigma_{mean}$) errors in the least significant digits. The plotted Pb-isotope data are not age corrected. Corrections to $^{208}Pb/^{204}Pb$, $^{207}Pb/^{204}Pb$ and $^{206}Pb/^{204}Pb$ ratios for basalts with average Th/Pb and U/Pb ratios of 0·633 and 0·137 would be –0·261, –0·008 and –0·172, respectively, at 132 Ma. For the quartz latites (average Th/Pb and U/Pb of 0·579 and 0·193) the corrections are –0·117, –0·006 and –0·119, respectively.

THE GOBOBOSEB MAFIC UNITS

Introduction

Comparison of TiO_2, Zr, Y, P, Nb and Sr abundances of the regional Etendeka LTZ (Tafelberg-type; Erlank *et al.*, 1984) and LTZ.L basalts from the southern Etendeka and Goboboseb Mountains, respectively (e.g. Figs 3–6), illustrate the existence of a previously unrecognized basaltic series, comprising both lavas and dykes, which possess higher MgO, TiO_2 and FeO* (total Fe as FeO), and a wider range of Ti/Y ratios. The newly recognized basalt series, the LTZ.H series, are distinguished by mineralogical, chemical and isotopic criteria from associated LTZ.L basalts (see below).

In the Goboboseb Mountains the majority of the LTZ.H basalts outcrop in the lower, northern part of the sequence, and one flow is interbedded between QL Units II and III. Chemically equivalent dykes are exposed in the northern and central Goboboseb. Outlying flows also occur at the base of the Awahab Formation type section in the Huab Valley, north of the Goboboseb (Fig. 1). The remaining basalts, including the Messum Mountain and Copper Valley flows, and associated dykes and plugs, are LTZ.L types and similar to the regional Tafelberg-type.

Classification and regional comparisons

Classification is based on the FM ratio [(FeO* + MnO)/(FeO* + MnO + MgO); expressed as wt % following the similar schemes of Carmichael (1964) and Wood (1978) for tholeiitic lavas of Iceland]. The classification scheme has been found appropriate for the majority of the Goboboseb mafic lavas and dykes; the small number of exceptions are noted as appropriate. Divisions are: High-Mg Basalt FM <55; Basalt FM 55–65; Low-Mg Basalt FM 65–74; Ferrobasalt FM 74–78; Basaltic Andesite FM 78–81; Icelandite FM >81. In addition, *mg*-number [mol % Mg/(Mg + ΣFe)] is used for some plots.

The Etendeka Province can be divided into northern and southern regions, a division which is based mainly on the relative abundances of Ti, Zr, P and high field strength elements (HFSE), and the isotopic characteristics of the mafic lavas and dykes. Volcanic successions to the north are characterized by interbedded high Ti–Zr (TiO_2 >2·5%; Zr >250 ppm; HTZ or Khumib-type) and the

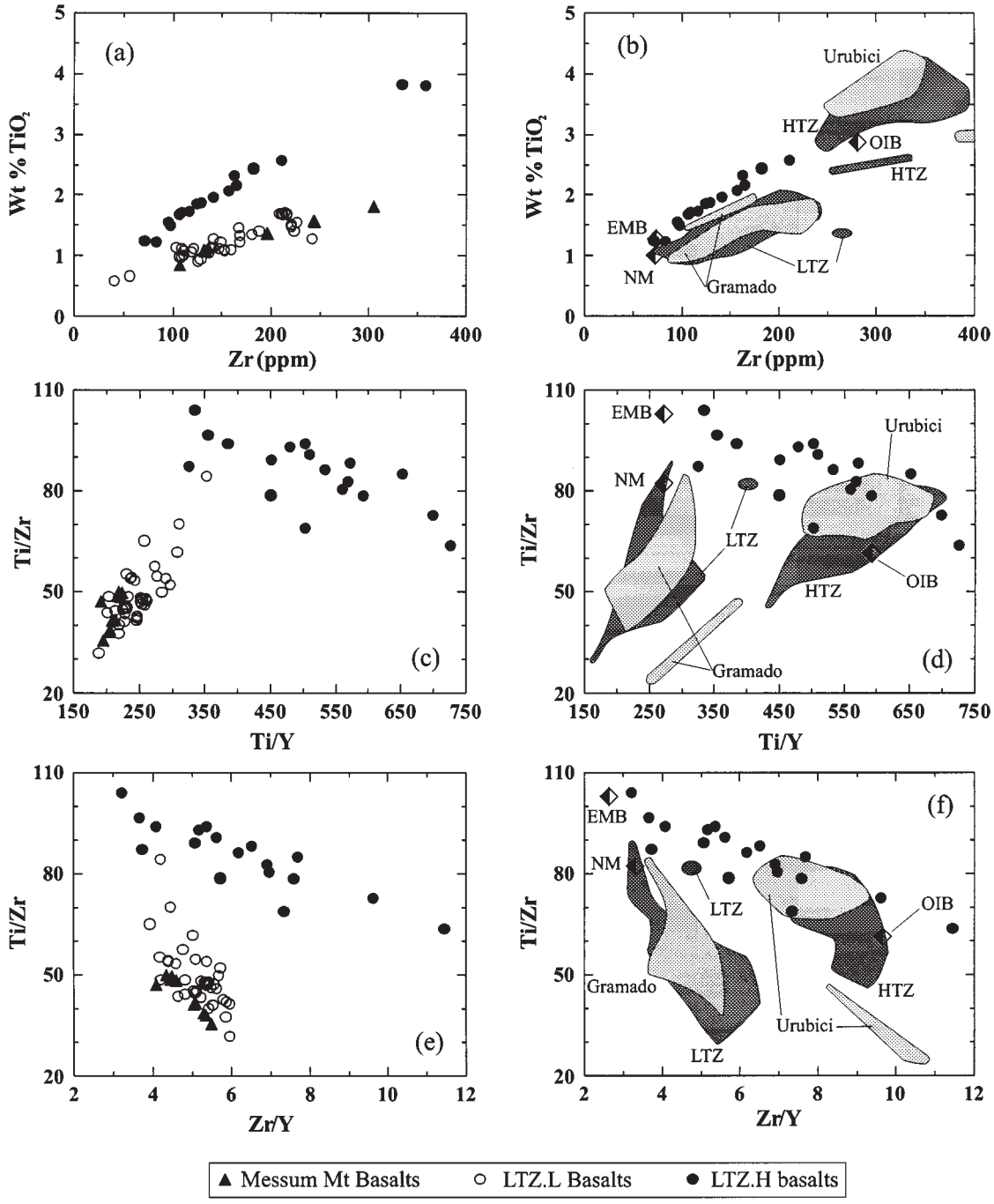

Fig. 3. Companion plots of TiO_2–Zr, Ti/Zr–Ti/Y and Ti/Zr–Zr/Y comparing the compositions of the Gobobosęb LTZ.H (shown in all plots) and LTZ.L basaltic series, with the Etendeka regional LTZ and HTZ series (Erlank *et al.*, 1984), and the Parana Gramado and Urubici series (Peate, 1989; Peate *et al.*, 1992). The average E-MORB (EMB), N-MORB (NM) and ocean island basalt (OIB) compositions are after Sun & McDonough (1989).

low Ti–Zr (LTZ or Tafelberg-type) basalts, whereas in the south the HTZ basalts are absent and mafic lava successions are dominated by LTZ magma types.

The Etendeka flood basalts are spatially associated with three main dolerite suites: (1) The Tafelberg dolerites (compositionally similar to the Tafelberg basalts; Erlank *et al.*, 1984); (2) the Horingbaai dolerites of the Southern Etendeka, similar chemically and isotopically to

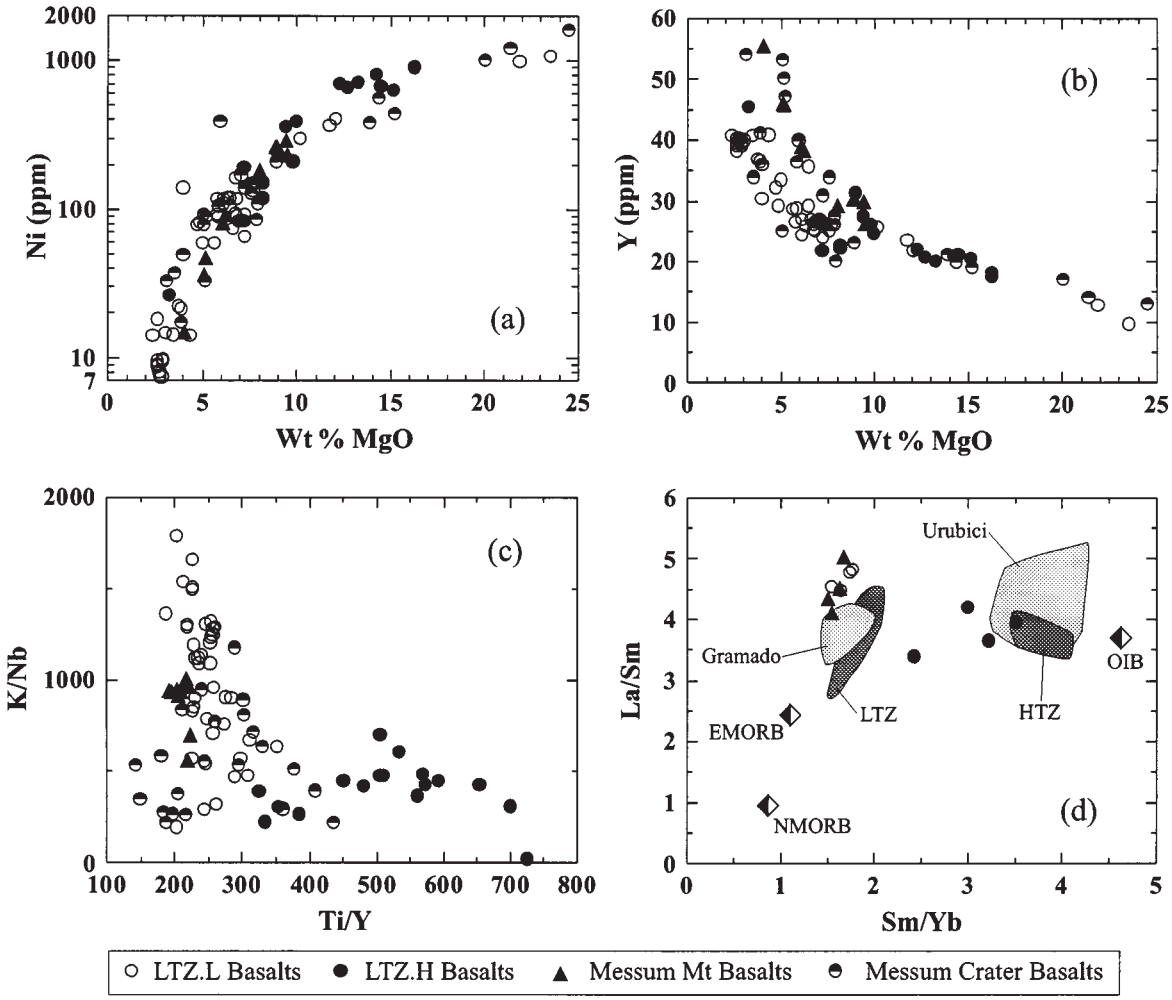

Fig. 4. Ni and Y vs MgO, K/Nb–Ti/Y and La/Sm–Sm/Yb plots of the Goboboseb LTZ.H, LTZ.L and the Messum Crater Basalts. In (d), comparative data from the regional Etendeka and Parana Gramado and Urubici series are shown (data sources as in Fig. 3 caption).

transitional mid-ocean ridge basalt (MORB) (Duncan *et al.*, 1990); (3) the Huab dolerites from the Huab River area (Fig. 1), comprising a complex of large sills with affinities to the Horingbaai dolerites, but differing in respect to ε_{sr}, Ti/Zr and Ba/Nb ratios (Duncan *et al.*, 1989).

In the Parana Basin, Peate *et al.* (1992) have revised the equivalent basaltic stratigraphy, although they still recognize the validity of the twofold 'Low-Ti' (<2 wt % TiO_2) and 'High-Ti' (>2 wt % TiO_2) groupings. Within their Low-Ti series are defined the Gramado, Esmeralda and Ribeira magma types, with the Etendeka Tafelberg-type (LTZ) series specifically equated with the Gramado type. The Parana High-Ti series are divided into the Urubici, Pitanga and Paranapanema types, with the Etendeka Khumib-type (HTZ) equated with the Urubici type. Stratigraphically, Peate *et al.* (1992) inferred the Urubici and Gramado lavas to interfinger and form the lowest part of the volcanic sequence, in accord with observed stratigraphy in the northern Etendeka.

Geochemical plots (e.g. Figs 3–5) confirm the very close affinities of the Parana Gramado and Urubici magma types with the Etendeka Tafelberg- and Khumib-type basalts, respectively. Moreover, these plots show that no previously documented extrusive equivalents to the Goboboseb LTZ.H basalts have been recognized from the Parana [see also Peate *et al.* (1990) and Peate & Hawkesworth (1996)].

Mineralogy

Phenocryst phases comprise ±olivine, augite and plagioclase, with Fe–Ti oxides and pigeonite appearing as

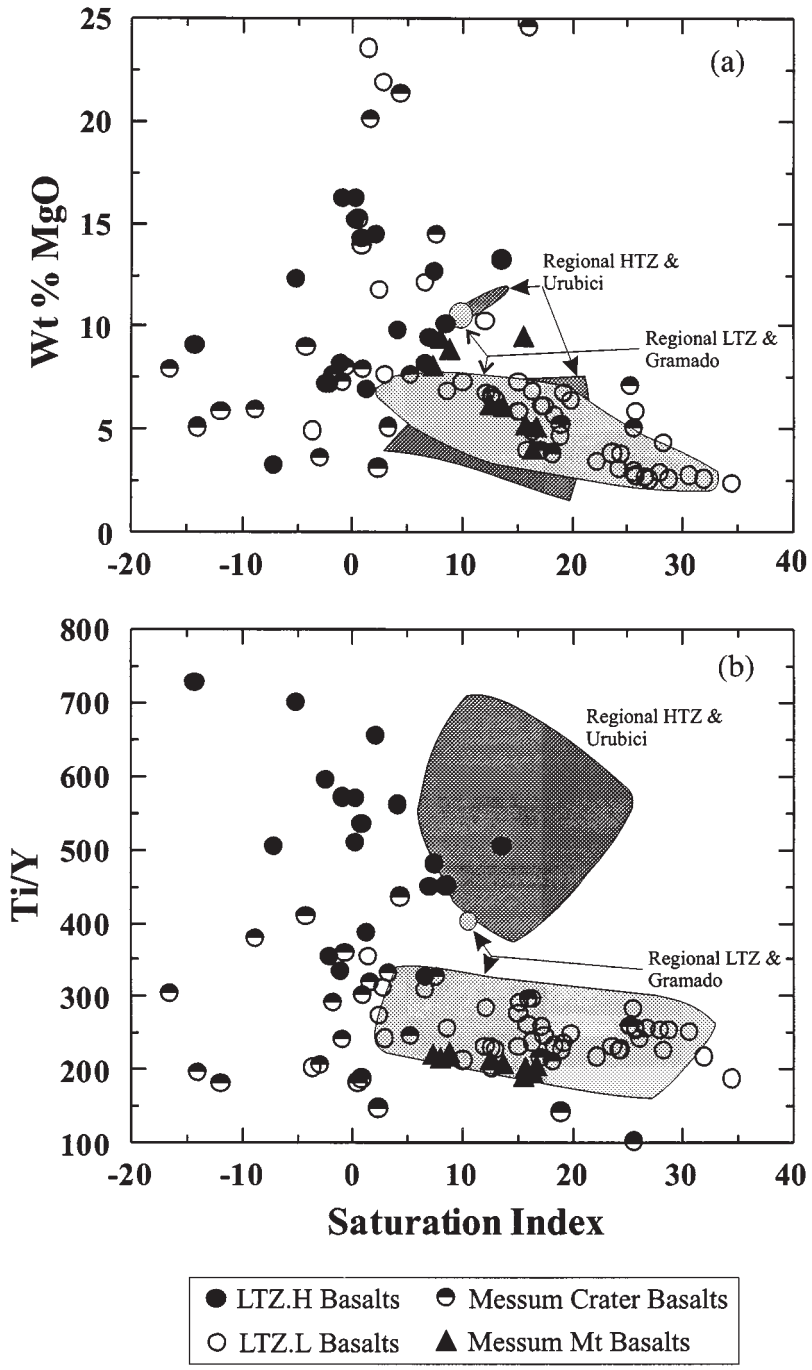

Fig. 5. Saturation index (Fitton *et al.*, 1991) vs MgO and Ti/Y, comparing the Goboboseb basaltic series with the regional Etendeka LTZ and HTZ, and Parana Gramado and Urubici series (data sources as in Fig. 3 caption). It should be noted that the Etendeka LTZ and Gramado, and the Etendeka HTZ and Urubici fields coincide sufficiently closely to be included as single fields, respectively.

microphenocrysts to phenocrysts in the ferrobasalts and icelandites. Table 2 summarizes the mineralogy of the two suites of Goboboseb extrusive and dyke phases.

LTZ.L-type lavas and dykes

These comprise a tholeiitic series ranging from high-Mg basalts to icelandites. Phenocryst assemblages vary with

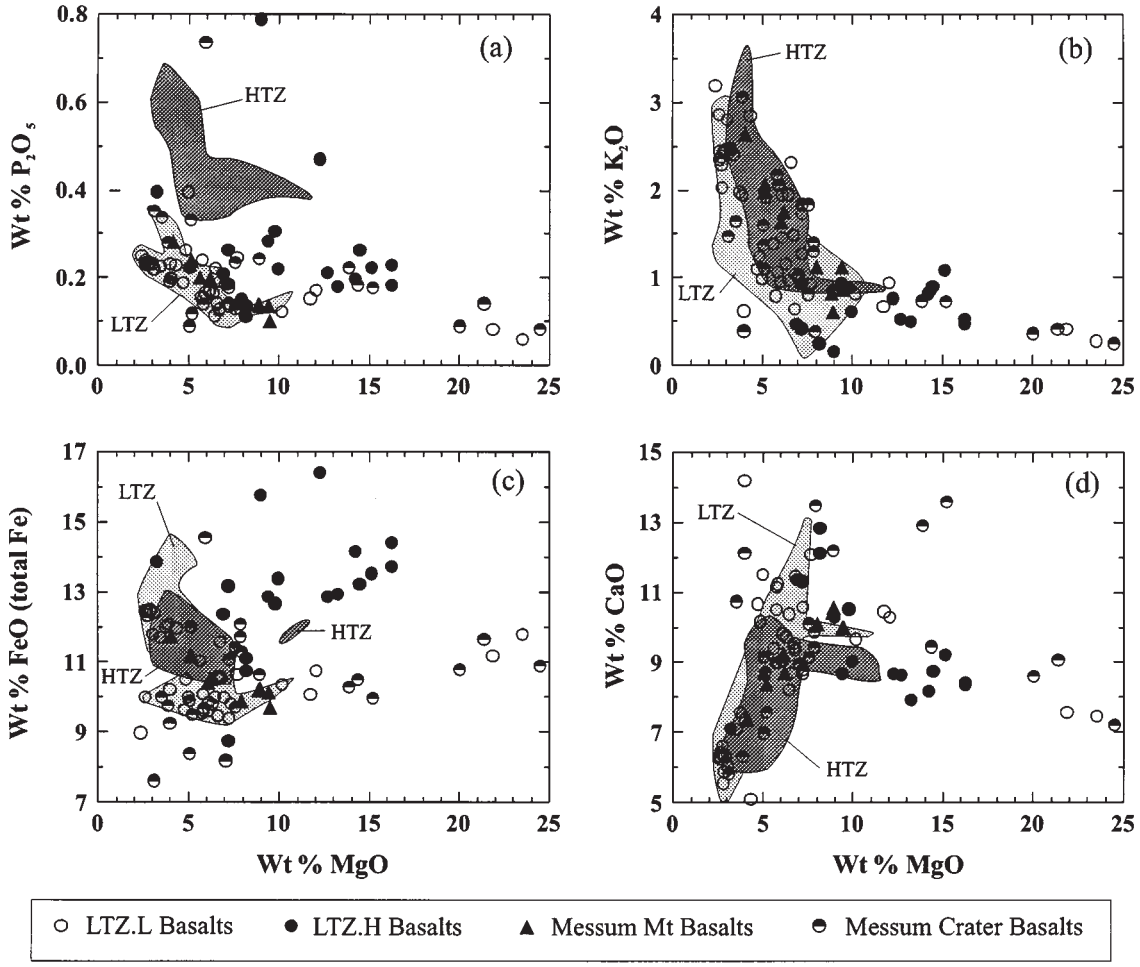

Fig. 6. P_2O_5, K_2O, FeO* and CaO vs MgO of the Goboboseb basaltic series compared with the regional Etendeka LTZ and HTZ series.

mg-numbers. Olivine ($Fo_{77–85}$), with rare Cr-spinel inclusions, occurs in low modal abundances ($\leq 3\%$) only in the most magnesian lavas. Plagioclase phenocrysts ($An_{56–79}$) are ubiquitous, commonly coexisting with augite and very rarely Cr-spinel. Augite (Fig. 7a–d) exhibits typical tholeiitic low-Ca compositions, extending to subcalcic types in the groundmass phases of some samples; limited Fe enrichment is developed, especially evident within the ferrobasalt, in which augite coexists with groundmass ferropigeonite.

Messum Mountain Basalts. These range from high-Mg basalts to ferrobasalt, uniformly aphyric to sparsely phyric. Plagioclase ($An_{54–69}$) occurs as rare microphenocrysts and groundmass microlites. Augite is the only groundmass pyroxene, and shows systematic changes in composition with changing whole-rock compositions (Fig. 7e).

Copper Valley Basalt. This is sparsely phyric and chemically a very homogeneous strictly icelandite lava, containing microphenocrysts and phenocrysts of plagioclase ($An_{49–61}$), pigeonite and rare ferroaugite (Fig. 7f and g), ilmenite and titanomagnetite, in a groundmass with a similar phase assemblage. Pyroxene temperatures are estimated to lie between 950 and 1120°C (Lindsley, 1983). The overall mineralogy reflects the Fe-enriched and more evolved composition of this unit.

LTZ.H-type lavas and dykes

Lavas and dykes of this series range from mildly alkaline (*ne*-normative) to tholeiitic (*hy*-normative). Olivine phenocrysts occur in all samples with $mg > 50$, ranging from $Fo_{64–85·8}$ (whole-rock *mg* ratios 64–68) to $Fo_{57–79}$ (whole-rock *mg* ratios 50–60), and phenocrysts of augite and plagioclase ($An_{30–66}$) occur in less magnesian samples.

Table 2: Phenocryst petrography and mineralogy of the Goboboseb mafic lavas and dykes

I. LTZ.L Series	
A. Tafelkop Lavas and associated dykes	
High-Mg basalts	Sparsely Oliv-phyric ($Fo_{77–85}$) + Cr-spinel ± Pl ($An_{56–70}$)
Basalts (*mg* > 53)	Either: (a) sparsely to moderately phyric with Pl (1–3%) + Oliv (1–3%) ± Cpx (1–3%), or (b) strongly phyric with Pl (10–25%) + Oliv (1–5%) ± Cpx (1–5%). Oliv: $Fo_{69–77}$; Pl: $An_{51–80}$
Basalts (*mg* < 53) and Low-Mg basalts	Either: (a) strongly phyric with Pl (10–15%) + Cpx (3–8%) ± Oliv (< 2%) ± Cr-spinel (Tr), or (b) sparsely phyric with Pl ± Cpx ± Fe–Ti oxides. Pl: $An_{62–79}$
Ferrobasalts and basaltic andesites	Sparsely phyric with Pl + Cpx ± Fe–Ti oxides. Pl: $An_{56–77}$
B. Copper Valley icelandite	
Icelandite	Sparsely phyric with microphenocrysts of Pl + rare pigeonite + Ti-mag + ilm in gmss of Pl + ferroaugite + ferropigeonite. Pl: mphen, $An_{46–61}$; gmss, $An_{44–60}$
C. Messum Mountain Basalts	
Basalts	Aphyric to sparsely phyric ranging from high-Mg basalts to ferrobasalts. High-Mg basalts contain very sparse phenocrystal Oliv + Pl. Remaining lavas contain rare phyric pl. Groundmass Pl microlites range from $An_{50–73}$ (high-Mg basalts), $An_{54–69}$ (basalts and low-Mg basalts), to $An_{54–63}$ (ferrobasalts)
II. LTZ.H Series	
Tafelkop lavas and dykes	
High-Mg basalts	Moderately to strongly phyric with Oliv (10–25%) ± Cpx (5–10%). Oliv: $Fo_{64–86}$; Pl: $An_{56–60}$
Basalts	Either: (a) sparsely phyric with Oliv, or (b) moderately to strongly phyric with Oliv (5–15%) ± Pl. Oliv: $Fo_{57–82}$; Pl: $An_{30–66}$
Low-Mg basalts	Either: (a) sparsely phyric with Pl + Ti-mag, or (b) strongly phyric with Pl (20–30%) + Cpx (1–3%) ± Oliv (<2%) ± Cr-spinel (Tr)
Ferrobasalts and basaltic andesites	Aphyric to sparsely phyric with Pl + Cpx ± Fe–Ti oxides

Pl, plagioclase; Oliv, olivine; Cpx, calcic clinopyroxene.

Pyroxene compositions (Fig. 7h–k) closely reflect the degree of whole-rock silica saturation, with the microphenocrysts and groundmass pyroxenes in the mildly alkaline high-Mg basalts exhibiting calcic and magnesian-augite compositions with little Mg–Fe variation. The more strongly *hy*-normative, high-Mg basalts and basalts contain less-calcic phenocrystal to groundmass augites, which in one high-Mg basalt sample coexist with groundmass pigeonite; the pyroxene temperatures estimated for this sample range between 1050 and 1200°C (1 bar; Lindsley, 1983). In the basalts, augite develops limited Fe enrichment in the groundmass and in phenocryst rims.

The most remarkable pyroxenes occur in a ponded, relatively evolved *ne*-benmoreite (phono-tephrite) lava, which outcrops at the northern limit of the Goboboseb Mountains. This rock, which formed during '*in situ*' fractionation, is a coarse-grained, mildly undersaturated rock, characterized by titanaugite which shows peripheral and gradational interstitial zoning to zirconian aegirine (Fig. 8). These pyroxenes exhibit a trend of increasing Zr with increasing Na substitution, presumably reflecting the coupled substitution $Zr^{4+} + Na^{+} = Ca^{2+} + Fe^{3+}$ (Fig. 8), with a maximum ZrO_2 of 12·7 wt % analysed (Table 3); the Na–Zr enrichment correlates with increasing Fe enrichment. Interstitial fluor-richterite is sporadically present. These data illustrate the trend, in the LTZ.H melts, towards the evolution of a peralkaline late stage residual liquid, in complete contrast to the mineralogy and chemistry of the evolved LTZ.L icelandites previously described. The chemistry of these evolved lavas therefore emphasizes the contrasting chemistries of the LTZ.H and LTZ.L magma series.

Messum Crater Basalts (MCB)

Some of these lavas are conspicuously porphyritic (augite, plagioclase, olivine and possibly orthopyroxene pseudomorphs). The fine-grained matrices commonly show modification by recrystallization, and, in some samples, by the introduction of fine veinlets of granitic melt. Rare amygdales and sandstone (?Karoo) xenoliths are present.

The augite phenocrysts are the most conspicuous mineralogical feature of the phyric lavas, possessing complex and delicate oscillatory zoning, but all optically clouded

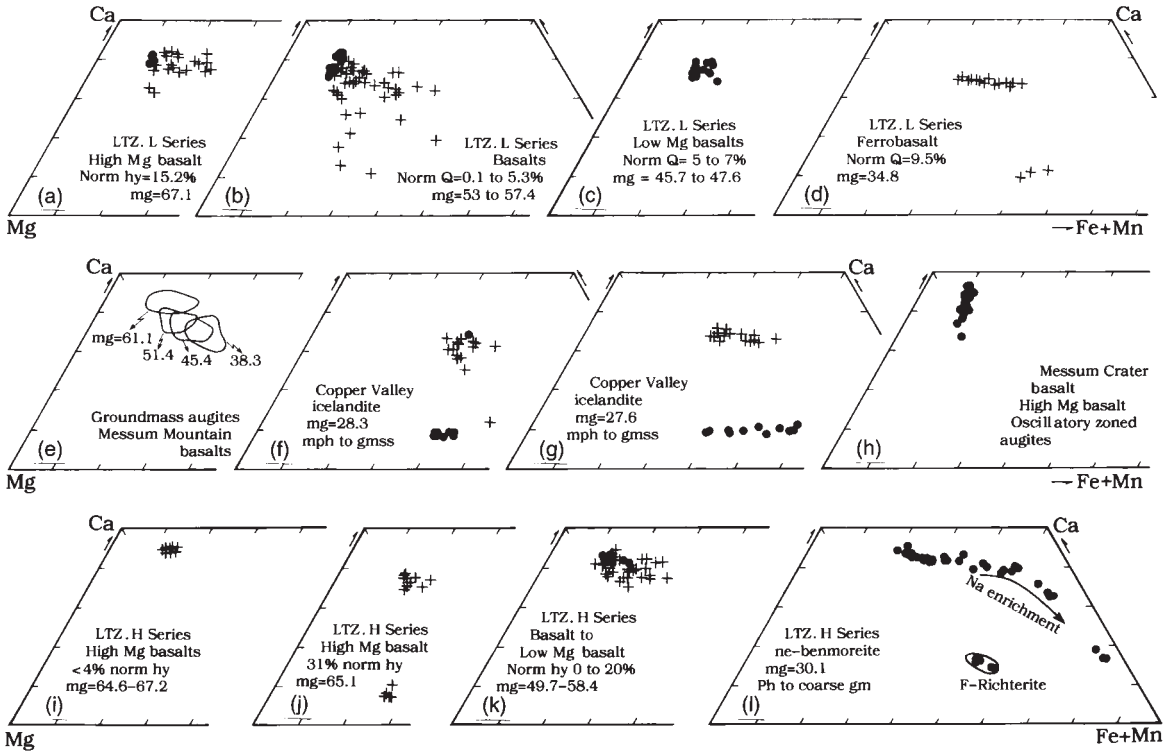

Fig. 7. Plots of the pyroxene phenocryst (●) and groundmass (+) compositions (mol.) in the Goboboseb mafic volcanics. In (e), the enclosed areas show the augite compositional fields from four lavas, for which the whole-rock *mg* ratios are listed. In (l), the coexisting richterite compositions are also shown; in this sample, both the pyroxene and richterite phases range between phenocryst and coarse groundmass.

Table 3: Selected aegirine to zirconian aegirine microprobe analyses from ponded ne*-benmoreite (phono-tephrite) lava, Northern Goboboseb (sample SMG126) (all values in wt %)*

SiO_2	49·45	48·97	49·37	49·24	49·54	49·79	49·30
ZrO_2	0·25	0·80	3·44	6·22	9·38	11·41	12·75
TiO_2	0·44	0·51	0·69	0·64	0·40	1·00	0·92
Al_2O_3	0·17	0·13	0·23	0·11	0·08	0·09	0·10
Fe_2O_3*	3·55	6·22	7·17	6·44	7·22	5·93	6·26
FeO*	22·81	20·08	18·12	18·10	16·35	16·33	15·75
MnO	0·41	0·30	0·27	0·27	0·25	0·18	0·13
MgO	4·38	3·61	2·60	1·79	1·39	0·88	0·47
CaO	18·48	16·95	13·36	10·44	8·24	4·70	3·51
Na_2O	1·07	2·36	4·64	6·07	7·64	9·27	9·92
Total	101·01	99·93	99·89	99·32	100·49	99·58	99·11

*Calculated on basis of O = 6 and Σ cations = 4.

by extremely fine dust-like exsolution products (Fig. 9). These textures suggest re-equilibration, apparently because of reheating of the lavas by later intrusive activity within the Messum Complex. Microprobe traverses across the phenocrysts reveal marked variations of Ca, Na and Al, although different crystals (even in one sample)

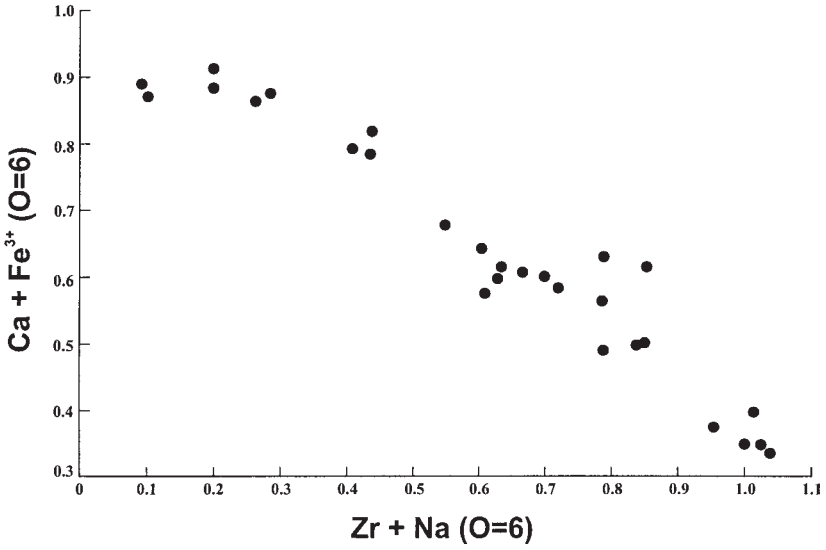

Fig. 8. Variation of Zr in the pyroxenes from the ponded *ne*-benmoreite (sample SMG126), expressed in terms of the coupled substitution of $Ca^{2+} + Fe^{3+} = Zr^{4+} + Na^{+}$. (See also Table 3.)

exhibit distinct patterns of zoning. The compositions (Fig. 7h) vary in Ca, but with little change of Mg–Fe ratios. Comparable textural and compositional variations have not been observed in Goboboseb mafic units. The pyroxene zoning patterns in the MCB are most plausibly thought to reflect magma mixing processes, involving LTZ.L and LTZ.H magmas; this is consistent with the variable and transitional chemistry of many of the MCB lavas (see below).

Bulk composition and phenocryst assemblages

To evaluate the significance of phenocryst assemblages, especially those phases considered as liquidus and near-liquidus phases, the whole-rock chemistries are plotted in the CMAS ($CaO–MgO–Al_2O_3–SiO_2$) projections from SiO_2 (Fig. 10), the data subdivided according to the phenocryst assemblages. This projection is relatively tightly constrained as it projects almost along the liquid line of descent from SiO_2.

The plots illustrate the contrasting phase assemblages and composition between the LTZ.L and LTZ.H magma series. The majority of LTZ.H-type lavas are silica undersaturated to just saturated (see also Fig. 5), the most silica-saturated sample ($mg = 65{\cdot}1$; *hy*-normative) containing groundmass pigeonite. As most of the LTZ.H samples lack phenocrystal plagioclase (pl) $\pm$ augite (cpx), they will not define cotectics. In contrast, the LTZ.L-type lavas are predominantly silica saturated, with normative *hy* and $\pm$Q. The LTZ.H lavas project as two overlapping and nearly linear arrays, the trajectories indicating either olivine (ol) or ol + cpx control, these two trends correlating with the observed presence or absence of cpx phenocrysts. Plagioclase saturation only develops in the most evolved compositions (*ne*-benmoreite). The LTZ.L lavas range from plagioclase unsaturated, through ol + pl, to cpx + pl assemblages with increasing normative plagioclase, with bulk chemistry and phenocryst assemblages well correlated. This is especially clear with respect to the Copper Valley and MMB lavas (Fig. 10c).

The major aspect shown by the data is the correlation of major element compositions with observed mineralogy and the projection of the data close to experimental low-pressure ol–cpx–pl–liquid cotectics (also well shown by the CMAS projection from plagioclase, not shown), consistent with the operation of relatively low-pressure (crustal) crystal fractionation processes.

Major and trace element compositions

The relatively magnesian compositions of the majority of the LTZ.H lavas are their most significant major element characteristic, as similarly magnesian compositions are rare in the regional flood basalts elsewhere in the Etendeka or Parana (Figs 5a and 6; Peate & Hawkesworth, 1996). Average MgO % of the LTZ.L basalts is $5{\cdot}38$ ($\sigma = 2{\cdot}16$; $n = 44$), contrasting with $11{\cdot}25$ ($\sigma = 4{\cdot}17$; $n = 13$) for the LTZ.H series. In the Goboboseb, only two analysed LTZ.L samples with higher MgO levels are known, both highly olivine-phyric (?cumulative) plugs (Fig. 6). Compared with the LTZ.L

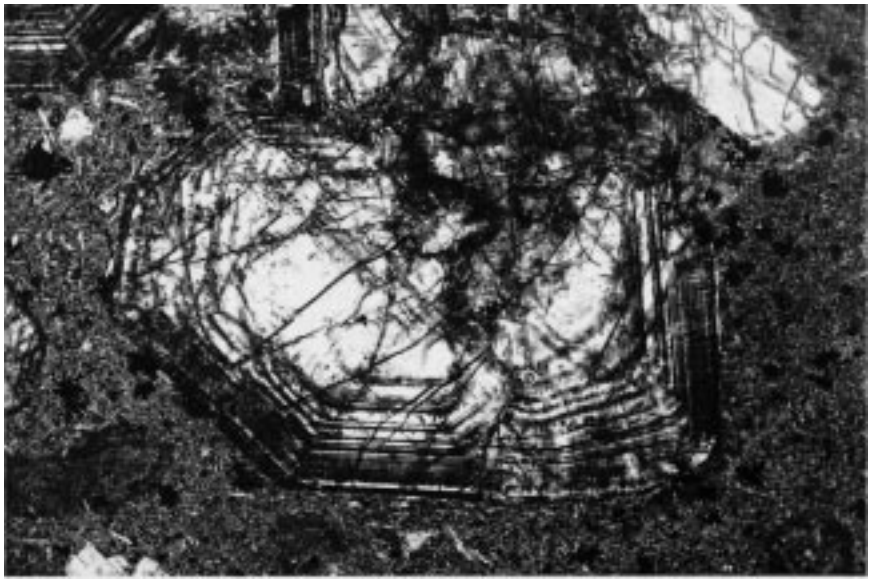

Fig. 9. Photomicrographs of intricately zoned and finely exsolved augite phenocryst in Messum Crater Basalt sample. Field of view 3·3 mm.

basalts, the LTZ.H magmas have higher abundances of FeO*, TiO_2, P_2O_5, Ni, Sr, Cu, Co and Cr, and generally lower K_2O, Rb and Sc (e.g. Figs 4 and 6). Element behaviour patterns of both basaltic series indicate significant crystal fractionation effects, although with differing trends. For example, Al_2O_3 and CaO (Fig. 6d) increase with decreasing MgO in the LTZ.H series, consistent with olivine-dominated fractionation (see also Fig. 10b), whereas the majority of the LTZ.L series exhibit decreasing CaO and Al_2O_3 with decreasing MgO, consistent with plagioclase fractionation ($\pm$ pyroxene and olivine). No simple correlation is observed between MgO–FeO* values (Fig. 6c), or MgO–Sc values, the differing abundance patterns between the two basaltic series being considered as source related. V–FeO* values are correlated in the LTZ.L series, but not within the LTZ.H lavas, pointing to significant Fe–Ti oxide fractionation in the LTZ.L magmas. Ni–MgO (Fig. 4a) and Cr–MgO are well correlated, and again imply control by olivine–clinopyroxene fractionation, most strongly developed in the LTZ.H series. K_2O is inversely correlated with MgO (Fig. 6b), and is therefore relatively higher in the LTZ.L basalts and dolerites, further illustrated by the K/Nb–Ti/Y plot (Fig. 4c).

Ti/Zr, Ti/Y and Zr/Y ratios (Fig. 3) not only clearly demarcate the two basaltic series, but define separate trends. To some degree the LTZ.H basalts appear to link the regional Etendeka LTZ (Tafelberg-type) and HTZ (Khumib-type) series, and these plots further suggest that the LTZ.H basalts span compositional space between MORB and OIB (Sun & McDonough, 1989), as also seen in other plots such as Zr–TiO_2 (Fig. 3) and Ba–Ti, Zr–P_2O_5 and Ti/Y–K/Nd (not shown). In contrast, Nb/La (~0·4–0·9), Nb/Th (~2–12), Nb/Pb (~2–9) and Nb/U (~4–55) tend to be generally lower than typical OIB or MORB ratios, although with some overlap. Figure 11b illustrates primitive mantle normalized spidergrams of three of the most magnesian LTZ.H basalts, and two of the most magnesian LTZ.L basalts, which emphasize the differences between the LTZ.H and LTZ.L magma but with the latter types showing relative enrichment in large ion lithophile elements (LILE), and depletions of Nb (strongest), P and Ti which are actually similar to arc patterns.

Rare earth elements (REE) (Table 4) within the more magnesian basalts differ between the two basaltic series. Although both are light REE (LREE) enriched, with overlapping La/Sm ratios (Fig. 4d), the heavy REE (HREE) are distinct, resulting in marked differences in Sm/Yb ratios (Figs. 4d and 11b). These differences are consistent with REE data for the regional Eteṇdeka LTZ and HTZ lavas and the corresponding Parana Gramado and Urubici types. The HTZ and Urubici types are close to OIB in terms of HREE fractionation. The LTZ.H series in fact bridge the compositions between the regional Etendeka LTZ and HTZ data, consistent with Ti/Y trends. A further important difference is the presence of consistent negative Eu anomalies (Eu/Eu* 0·83–0·94) in the LTZ.L basalts, indicative of plagioclase fractionation. The HREE differences are potentially significant as they suggest that the LTZ.H magmas were derived from the garnet stability zone, in contrast to the LTZ.L melts.

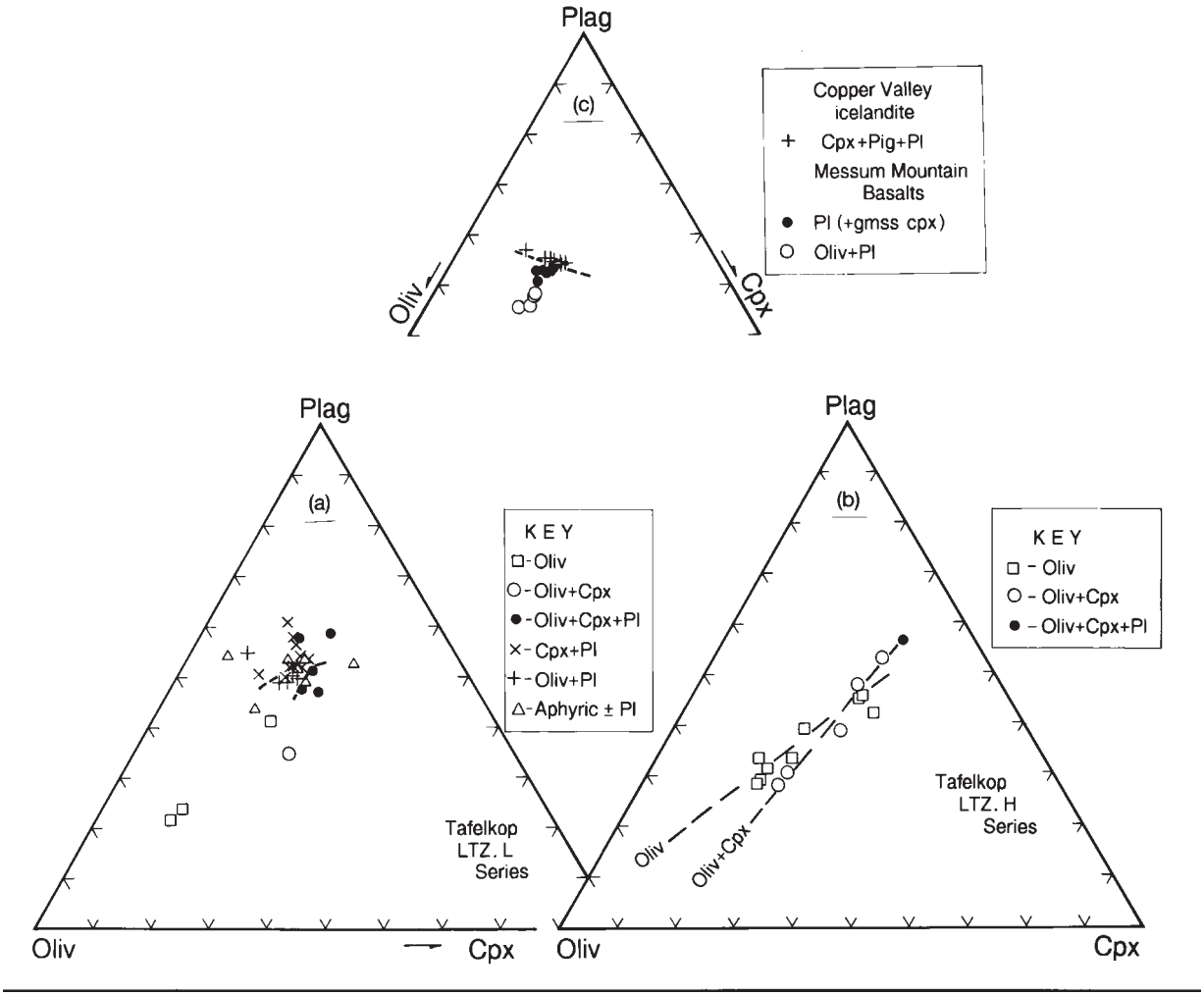

Fig. 10. CMAS projection from SiO_2 (after Walker *et al.*, 1979) of the Goboboseb mafic lava and dyke compositions, subdivided according to phenocryst assemblages. The dashed boundary lines in (a) and (c) are based on the observed changes in phenocryst assemblages, whereas in (b) they illustrate the oliv and oliv + cpx control trends (also based on observed phenocryst phases).

Such an interpretation in turn suggests a subcontinental lithospheric mantle (SCLM) thickness either in the garnet stability field, or at the garnet–spinel transitional zone, at the time of inferred plume impact.

Messum Mountain Basalts

The Messum Mountain Basalt sequence comprises a distinct stratigraphic package showing strongly coherent major and trace element variation trends (e.g. Figs 3 and 5), which are further illustrated (Fig. 11a) by E-MORB normalized spidergrams for four samples of progressively decreasing *mg*-numbers. The four patterns are very similar and exhibit increasing absolute element abundances that correlate with the decreasing *mg*-numbers. Systematic increases in ΣREE (Table 4), increasing La/Yb (from 6·3 to 8·4) and decreasing Eu/Eu* (from 0·94 to 0·85) ratios also correlate with the decreasing *mg* ratios. Although the geochemical behaviour is consistent with crystal–liquid fractionation, AFC behaviour is indicated by isotope data (discussed below). Notwithstanding the open system condition, the tight coherence of the trends points to a single line of descent, probably within a single interconnected magma chamber system.

Messum Crater Basalts

Representative plots (Figs 4–6) show that the basalts extend from 3 to 24% MgO, the most magnesian samples being olivine ± clinopyroxene phyric. They range between silica undersaturated and saturated (Fig. 5). In

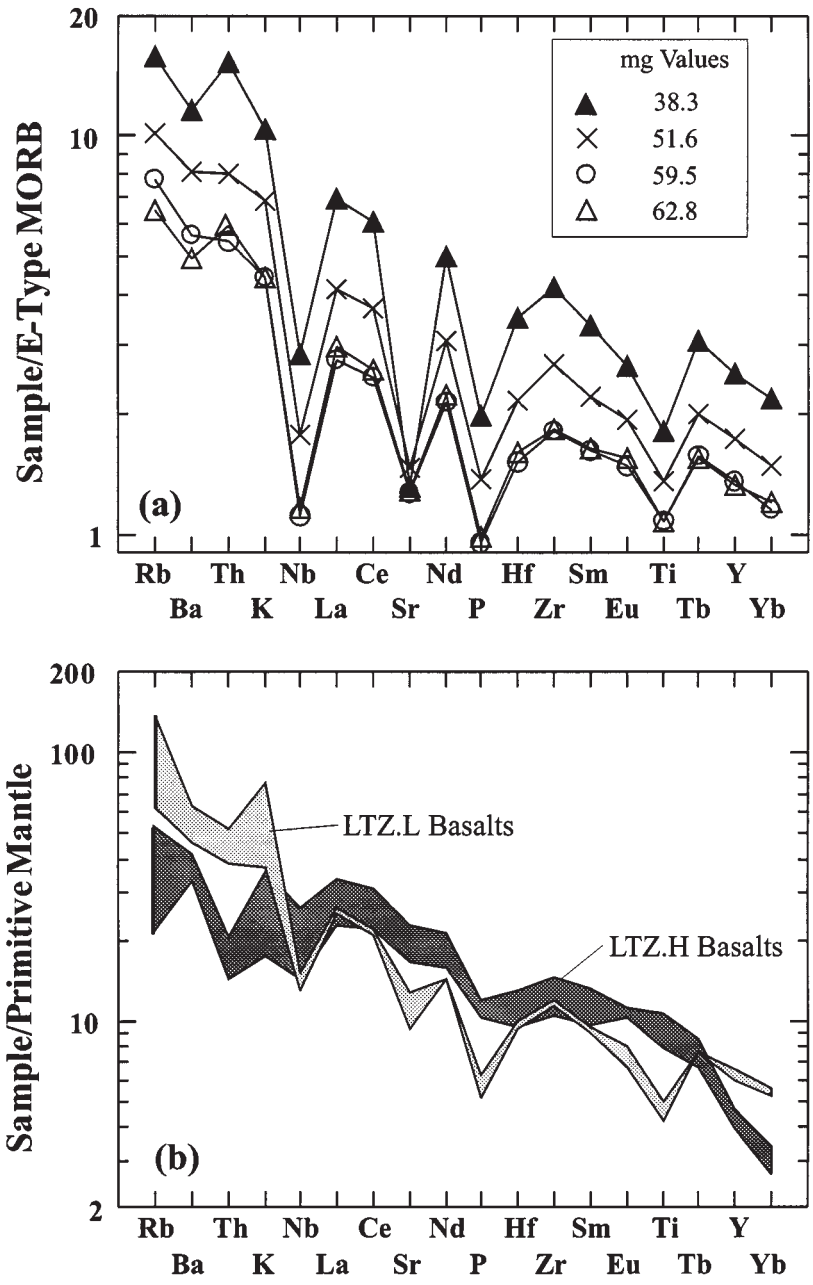

Fig. 11. (a) E-MORB normalized (Sun & McDonough, 1989) Messum Mountain Basalts samples, illustrating regular change of element abundances with changing *mg* values. (b) Primitive mantle normalized (Sun & McDonough, 1989) patterns for the most magnesian analysed Goboboseb LTZ.H and LTZ.L basalts.

terms of affinities with the LTZ.L and LTZ.H lavas, the MCB compositions overlap the major and trace element compositional fields of the LTZ.L-type (e.g. Fig. 6c), but a significant proportion overlap the two magma series, with a small number lying clearly within the LTZ.H compositional fields (Fig. 4b and c). The occurrence of lavas with apparently both LTZ.H and LTZ.L affinities within the Messum Complex strengthens the interpretation that Messum was a local eruptive centre for these lavas (although not necessarily the sole source), and further suggests that both magma types were existing simultaneously beneath the Messum volcanic centre.

Table 4: Major and trace element data for selected mafic lavas from the Goboboseb Mountains

Group:	LTZ.H Series				LTZ.L Series							
								Copper Valley	Messum Mt Basalt			
Sample:	SMG105	SMG016	SMG027	SMG127	SMG018	SMG024	SMG097	SMG032	SMG052	SMG053	SMG054	SMG057
SiO_2 (wt %)	46·39	45·77	49·99	47·44	52·97	54·02	54·19	58·44	54·44	52·46	50·33	50·08
TiO_2	1·95	1·72	1·85	2·31	1·22	0·91	1·07	1·71	1·81	1·36	1·08	1·08
Al_2O_3	10·44	10·31	12·26	10·27	17·68	15·45	15·44	13·22	14·90	16·29	16·85	15·87
FeO*	13·52	14·39	13·37	13·20	9·53	9·43	9·77	12·42	11·85	10·53	9·92	10·11
MnO	0·20	0·19	0·17	0·20	0·15	0·15	0·16	0·17	0·20	0·16	0·16	0·16
MgO	15·18	16·25	9·96	14·44	4·77	6·63	6·35	2·61	4·06	6·20	8·03	9·43
CaO	9·18	8·39	9·01	8·75	10·66	8·71	9·72	6·26	7·35	8·69	10·09	9·99
Na_2O	1·84	2·24	2·58	2·25	1·74	2·28	1·99	2·58	2·47	2·37	2·28	2·03
K_2O	1·08	0·52	0·61	0·90	1·09	2·31	1·15	2·35	2·64	1·75	1·11	1·11
P_2O_5	0·22	0·23	0·22	0·26	0·19	0·11	0·16	0·24	0·28	0·20	0·14	0·14
Trace elements (ppm)												
Rb	33·3	13·4	13·0	28·1	32·1	87·2	46·9	88·6	79·8	51·3	32·7	39·4
Ba	293	231	183	236	695	440	262	440	657	462	280	321
Sr	349	479	369	416	302	267	201	197	203	228	200	198
Th	1·6	1·2	1·0	1·7	4·2	4·4	4·8	8·6	9·2	4·8	3·6	3·3
U	0·62	0·20	0·21	0·82	0·64	0·92	1·0	2·1	0·82	0·41	0·41	0·21
Zr	142	117	125	163	169	126	153	215	305	195	134	133
Hf	3·4	2·9	2·9	4·0	3·8	2·9	3·6	5·3	7·1	4·4	3·3	3·1
Nb	18·7	10·1	11·3	17·4	11·0	10·7	12·3	15·8	23·5	14·8	9·7	9·2
Ta	1·3	1·1	0·82	1·7	1·2	1·1	1·1	1·7	2·05	1·3	0·82	0·92
Cr	911	736	575	1160	219	219	213	9·3	6·7	36	103	401
V	373	310	275	368	229	236	254	318	245	245	233	251
Sc	26	21	20	23	32	36	40	34	28	30	27	31
Ni	630	893	387	670	78	74	121	9·5	15	92	185	294
Co	91	99	76	86	41	50	48	43	43	49	56	58
Pb	4·0	1·4	1·6	2·6	3·1	3·1	3·1	4·4	4·7	4·0	2·5	2·2
Zn	128	117	121	100	94	87	94	109	115	112	90	91
Cu	107	120	111	168	80	51	94	50	23	49	73	81
Y	20·5	18·0	24·6	21·2	32·2	27·0	25·9	40·3	55·5	38·2	29·2	29·9
La	21·2	15·5	15·0	23·2	22·4	18·1	20·4	32·8	43·7	25·9	18·6	17·3
Ce	47·6	38·6	34·9	55·4	49·1	38·8	42·4	70·1	91·1	55·3	38·8	37·0
Nd	24·3	21·3	19·9	28·9	25·1	19·2	20·4	34·4	44·7	27·6	20·2	19·2
Sm	5·1	4·3	4·4	5·8	5·0	4·0	4·3	6·8	8·7	5·7	4·3	4·2
Eu	1·7	1·8	1·6	1·9	1·5	1·1	1·3	1·9	2·4	1·8	1·4	1·4
Gd	5·3	4·2	5·0	5·2	5·3	4·3	4·9	6·9	8·4	6·3	4·9	4·6
Tb	0·78	0·72	0·77	0·93	0·94	0·82	0·82	1·3	1·6	1·1	0·82	0·83
Ho	0·72	0·65	0·81	0·92	1·10	0·87	0·87	1·4	1·8	1·25	0·97	0·95
Yb	1·7	1·3	1·8	1·7	3·1	2·6	2·5	3·8	5·2	3·5	2·9	2·7
Lu	0·23	0·18	0·26	0·223	0·45	0·38	0·36	0·56	0·74	0·51	0·41	0·40
Eu/Eu*	1·01	1·28	1·06	1·02	0·89	0·83	0·86	0·83	0·85	0·89	0·94	0·93

All data recalculated on anhydrous basis, with ΣFe as FeO. Major elements, Rb, Ba, Sr, Zr, Nb, Cr, V, Sc, Ni, Co, Zn, Cu, Y and Pb (in part) by X-ray fluorescence (Department of Earth Sciences, University of Cape Town). Pb by atomic absorption graphite furnace (see Ewart *et al.*, 1994). Remaining trace elements by instrumental neutron activation analysis (B. W. Chappell, Australian National University). Methods as described by Chappell & Hergt (1989).

Isotope geochemistry

New Sr, Nd and Pb isotopic data (Table 5) point to the following relationships (Figs 12–14). It should be noted that these plots, and the following discussion, also include the associated silicic eruptives (see Part II), which are integral to these interpretations.

(1) The LTZ.H and LTZ.L magma series are isotopically distinct, reinforcing the previously described mineralogical and chemical differences. In Sr–Nd isotopic space, the LTZ.H compositions are closest to Atlantic MORB, projecting between the latter and the Walvis Ridge fields, whereas the LTZ.L series, in contrast, plot towards the quartz latite compositions in what is commonly regarded as a 'crustal' field in Nd–Sr space.

(2) Pb isotopic compositions of the LTZ.H basalts plot as relatively linear arrays. Alternative explanations for these arrays are that they represent either a secondary isochron, with an implied fractionation event at ~2·6 Ga, or mixing relations, plausibly either between Walvis Ridge and LTZ.L magmas ($^{207}Pb/^{204}Pb$–$^{206}Pb/^{204}Pb$), or more likely involving input of an Atlantic MORB component ($^{208}Pb/^{204}Pb$–$^{206}Pb/^{204}Pb$, $^{143}Nd/^{144}Nd$–$^{206}Pb/^{204}Pb$ and $^{87}Sr/^{86}Sr$–$^{206}Pb/^{204}Pb$ relations). Even this explanation is problematic as the LTZ.H lavas evidently do not define a simple MORB–Walvis Ridge mixing trend, which seems to require a third, more radiogenic Pb and Sr end member, possibly similar to the LTZ.L lavas. The $^{207}Pb/^{204}Pb$–$^{206}Pb/^{204}Pb$ data for the Etendeka MORB-like Horingbaai dolerites indicate these melts to be unlikely end members.

The preferred explanation is that the LTZ.H series represent magmas emanating from the inferred 130 Ma asthenospheric plume source (now seen at Tristan da Cunha and in the Walvis Ridge), inferred to have initially existed beneath the present NW Namibian coast (e.g. O'Connor & le Roex, 1992). The least radiogenic end of the LTZ.H Pb isotope arrays is therefore inferred to represent the closest approach to the original plume end member component. The arrays themselves are believed to be mixing controlled, involving two or possibly three components (see later discussion), and attention is drawn to the fact that the Pb–Nd–Sr isotopic compositions are similar to, but not identical with the modern Tristan compositions (whose compositions could well have undergone evolution over 130 Ma; e.g. Gibson *et al.*, 1995; Peate & Hawkesworth, 1996). This interpretation is consistent with that advocated by Milner & le Roex (1996) to explain the isotopic compositions of the alkaline gabbro suite in the Okenyenya igneous complex, whose isotopic compositions are similar to the LTZ.H basalts.

(3) The LTZ.L basalts exhibit evolved Nd–Sr isotope signatures, suggesting crustal mixing or AFC-type processes, but their compositions overlap those of both the regional Etendeka LTZ-type and the Parana Gramado basalt series (Fig. 12). The Pb isotopes of the LTZ.L basalts (Fig. 13) are also relatively radiogenic and again overlap with the main grouping of regional Etendeka LTZ and the Parana Gramado basalts. Hawkesworth *et al.* (1984), Hergt *et al.* (1991) and Peate & Hawkesworth (1996) have argued that low-Ti Gondwana CFB (including the Etendeka LTZ-type and the Parana Gramado series) were derived from geochemically distinctive sources in the SCLM which had previous depletion and enrichment histories, including the possible introduction of a minor subducted sediment component (see Duncan, 1987). It is therefore relevant to note the 1/Sr vs $^{87}Sr/^{86}Sr$, and 1/Nd vs $^{143}Nd/^{144}Nd$ plots (Fig. 15), in which the Sr data define a near-linear array (excepting the latite and rhyolite clasts within the Messum Core breccias), whereas the Nd data are more complex, with one possible trend between the LTZ.L and quartz latite magmas, and a second and separate trend for the LTZ.H magmas, possibly between an OIB-like component (?plume related) and lower crust. This trend appears unrelated to the Horingbaai dolerites (MORB-like), or the proposed Parana SCLM compositions (Gibson *et al.*, 1995). The data for the relatively evolved LTZ.L lavas (notably the Copper Valley icelandite and the Messum Mountain low-Mg basalts and ferrobasalt) are also characterized by more radiogenic Sr and less radiogenic Nd than the more Mg-rich LTZ.L lavas (Table 5). These relationships imply mixing and/or AFC involving crustal input, supported also by the strong positive correlation of ε_{Sr} with SiO_2 (Fig. 16; excepting again the Messum Core breccias).

(4) Although discussed in detail in Part II of this paper, it is noted here that the Springbok and Goboboseb quartz latites define the 'crustal' end of the Sr–Nd–Pb isotope data arrays, having relatively radiogenic Pb and Sr which overlap the isotopic compositions of the more 'evolved' LTZ.L lavas.

DISCUSSION

Plume and LTZ.L melts

Data presented clearly define two mafic lava types. The LTZ.H type is here identified as plume-dominated (i.e. Tristan plume) melts, although noting a degree of isotopic variability, believed to be mixing related. The lavas are relatively magnesian and olivine-phyric, and in one case have fractionated (at surface) to an *ne*-benmoreite (phonotephrite) derivative. Geochemically, they show transitional characteristics between E-MORB and OIB magmas. Exact correlations have not been recognized elsewhere in the main Etendeka lava field, with the exception of a flow south of the Huab River (Fig. 1), which may represent a remnant of the Goboboseb sequence. The LTZ.H and LTZ.L lavas are intercalated

Table 5: Sr, Nd and Pb isotopic analyses of Goboboseb mafic lavas

Sample	$^{87}Sr/^{86}Sr$	ppm Rb	ppm Sr	$(^{87}Sr/^{86}Sr)_0$	ε_{Sr}	$^{143}Nd/^{144}Nd$	ppm Sm	ppm Nd	$(^{143}Nd/^{144}Nd)_0$	ε_{Nd}	$^{206}Pb/^{204}Pb$	$^{207}Pb/^{204}Pb$	$^{208}Pb/^{204}Pb$
LTZ.H mafic lavas													
SMG105	0·705513±10	33·3	349	0·704984	6·15	0·512755±10	5·07	24·3	0·512644	3·61	18·733±5	15·660±5	38·602±5
SMG016	0·704818±10	13·4	479	0·704662	1·59	0·512617±10	4·26	21·3	0·512510	1·00	18·149±5	15·537±5	38·127±5
SMG027	0·705178±10	13·0	369	0·704983	6·13	0·512646±10	4·42	19·9	0·512528	1·34	18·362±6	15·580±6	38·344±6
SMG127	0·704553±10	28·0	416	0·704179	−5·28	0·512885±10	5·84	28·9	0·512777	6·21	18·781±5	15·629±5	38·313±5
LTZ·L mafic series													
SMG018	0·710638±10	32·0	302	0·710049	78·0	0·512132±10	5·02	25·1	0·512025	−8·46	18·711±5	15·701±5	39·115±6
SMG024	0·710458±50	87·2	267	0·708644	58·1	0·512255±10	3·98	19·2	0·512144	−6·14	19·039±4	15·695±4	39·209±4
SMG097	0·712950±10	46·9	201	0·711659	100·9	0·512235±10	4·29	20·4	0·512123	−6·56	18·899±5	15·707±5	39·228±5
Copper Valley flow													
SMG032	0·716178±20	88·6	197	0·713683	129·6	0·512163±10	6·81	34·3	0·512057	−7·84	18·853±6	15·701±6	39·046±6
Messum Mt Basalt													
SMG052	0·719018±40	79·8	203	0·716834	174·4	0·512078±10	8·70	44·7	0·511974	−9·46	18·651±6	15·690±6	39·149±6
SMG053	0·715148±40	51·3	228	0·713901	132·7	0·512135±10	5·74	27·6	0·512024	−8·49	—	—	—
SMG057	0·713768±10	39·4	198	0·712661	115·1	0·512166±10	4·21	19·2	0·512049	−8·00	18·673±6	15·681±6	39·147±6

Initial ratios and epsilon values corrected to 132 Ma. Analyst: R. A. Armstrong.

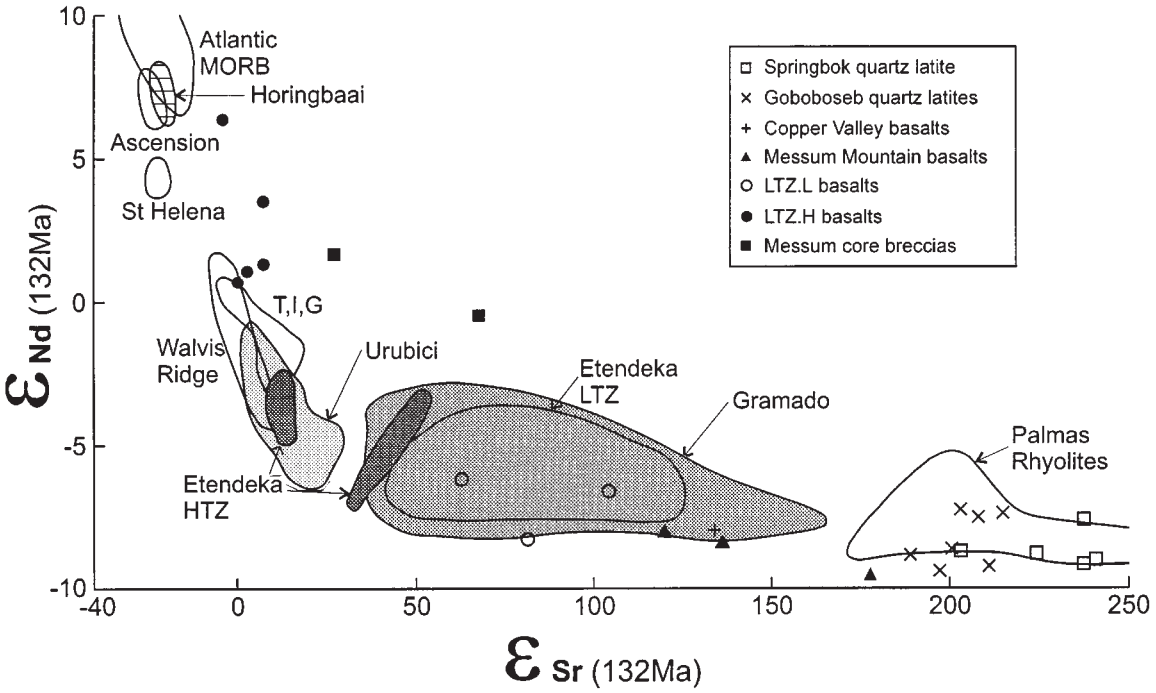

Fig. 12. ε_{Nd}–ε_{Sr} (132 Ma) of the Goboboseb LTZ.H and LTZ.L basaltic series, the Springbok and Goboboseb quartz latites (see Part II) and Messum Core breccias, compared with the compositional fields for other regional Etendeka and Parana lavas, plus Atlantic MORB, OIB [including Tristan da Cunha, Inaccessible and Gough Islands (TIG)] and Walvis Ridge data. Data sources: O'Nions & Pankhurst, 1974; O'Nions *et al.*, 1977; Cohen *et al.*, 1980; Dupre & Allegre, 1980; Cohen & O'Nions, 1982; Harris *et al.*, 1982; Richardson *et al.*, 1982, 1984; Weis, 1983; Hawkesworth *et al.*, 1984; le Roex, 1985; le Roex *et al.*, 1990; Garland *et al.*, 1995; Milner & le Roex, 1996.

within the lower northern part of the Tafelkop sequence, and are believed to represent eruption through an extending but still relatively rigid crust, before the main phase of crustal thinning and fusion (see Part II). An LTZ.H lava also occurs between the Goboboseb QL units and we assume represents final evacuation from an upper-crustal magma chamber. Milner & Le Roex (1996), however, have reported isotopically similar alkaline gabbros in the Mesozoic Okenyenya igneous (subvolcanic) complex, lying some 100 km ENE of Brandberg, which they interpret as Tristan plume derived also.

The LTZ.L lavas are more enigmatic, but are indistinguishable from the regional LTZ basaltic magma series. They fractionate to icelandite-type derivatives, are isotopically more 'evolved' than the LTZ.H types (trending towards EM-2 crustal compositions), are mineralogically characterized by groundmass pigeonitic and subcalcic pyroxenes, and have undergone pl + cpx + ol fractionation, implying crustal pressures. These lavas are therefore less magnesian than the LTZ.H series, which has implications for hidden cumulates, particularly considering their regional scale (Cox, 1993; Farnetani *et al.*, 1996). The LTZ.L lavas further exhibit consistent negative Eu/Eu* anomalies, higher K and Rb, and lower Ba, Ti, P, and Ti/Zr, Sm/Yb and Ti/Y ratios relative to the LTZ.H types. Apart from Eu, these features cannot be simply attributed to fractionation, and the LTZ.L and regional LTZ melts are interpreted to represent distinct magma series. One aspect of the LTZ.L geochemistry is the existence of 'arc-like' geochemical signatures as described originally by Duncan (1987), and is clearly shown by such plots as Th/Yb–Ta/Yb, Ba/Nb–La/Nb and Th/Ta/Hf (see also Fig. 11). These signatures are not present in the LTZ.H magmas, and suggest that the LTZ.L sources have experienced a prior arc 'overprint', consistent in principle with SCLM and/or crustal source contributions, and plausible in terms of the inferred Proterozoic Damaran history of the region (e.g. Henry *et al.*, 1990). The major problem is, however, the wide regional occurrence of these geochemical characteristics (Duncan, 1987), which extend well beyond the Damaran influence in southern Africa, although the possible lateral extent and influence of a large plume may offer an explanation for this (White & McKenzie, 1989). The LTZ Etendeka regional series are, therefore, widely interpreted as being predominantly derived from the SCLM (e.g. Cox *et al.*, 1984; Hawkesworth *et al.*, 1984, 1992; Hergt *et al.*, 1991; Peate & Hawkesworth, 1996). Milner

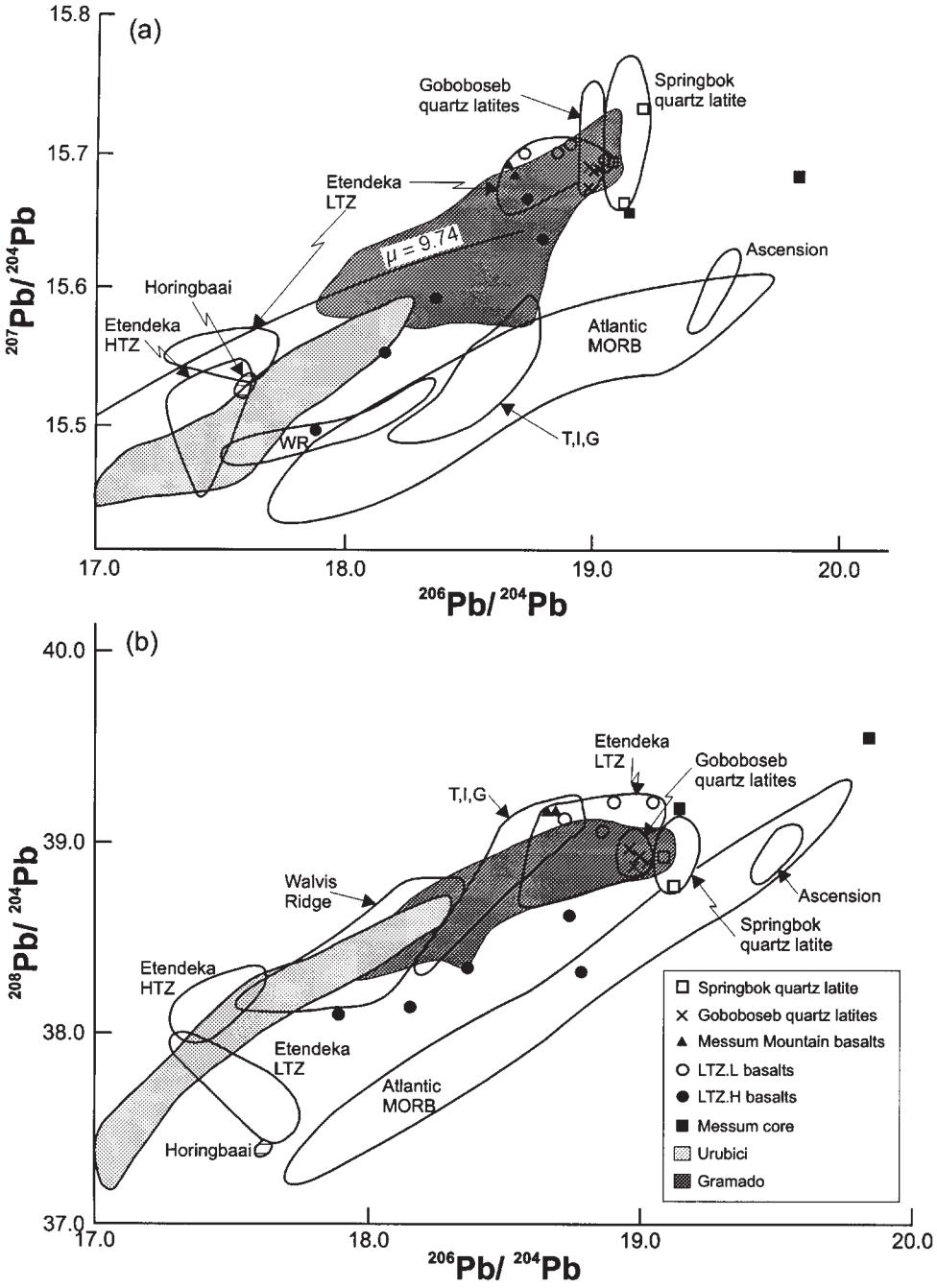

Fig. 13. Pb isotopic compositions of the Goboboseb LTZ.H and LTZ.L basaltic series, the Springbok and Goboboseb quartz latites and Messum Core breccias compared with the fields for the compositional fields of regional Etendeka and Parana lavas, plus Atlantic MORB, OIB [including Tristan da Cunha, Inaccessible and Gough Islands (TIG)] and Walvis Ridge compositions. Data sources as in Fig. 12 caption.

& le Roex (1996), however, suggested that their wide range of isotopic compositions is attributable to extensive crustal contamination, and Peate & Hawkesworth (1966) also acknowledged that variable upper-crustal contamination has modified the equivalent Gramado magma type of the Parana.

Rather than accepting an entirely SCLM origin for the Etendeka LTZ and LTZ.L melts, we try to evaluate

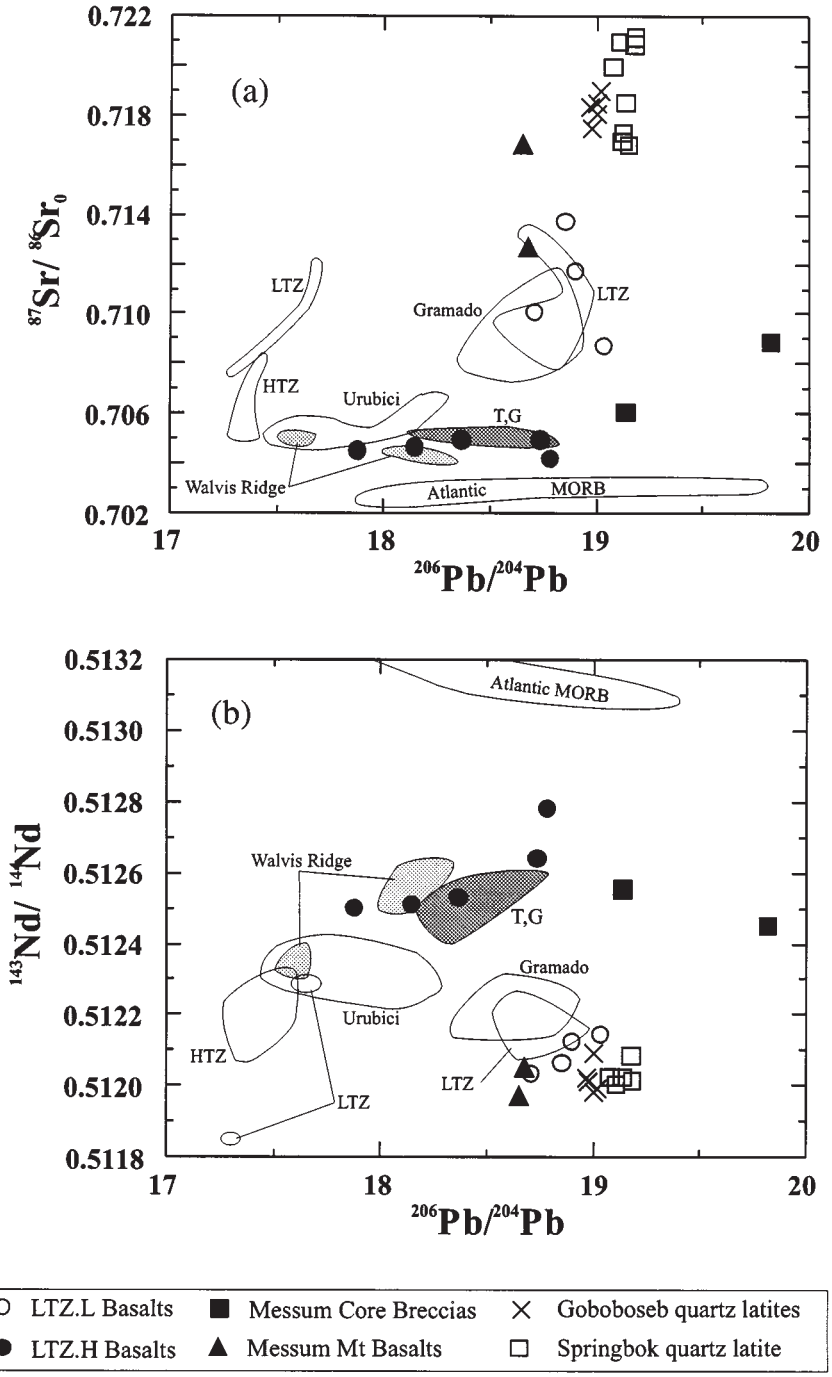

Fig. 14. Sr–Pb and Nd–Pb isotopic composition of the Goboboseb LTZ.H and LTZ.L basaltic series, the Springbok and Goboboseb quartz latites and Messum Core breccias, compared with the compositional fields of the Etendeka (LTZ and HTZ) and Parana (Gramado and Urubici) lavas, plus Atlantic MORB, Tristan da Cunha and Gough (T, B), and Walvis Ridge compositions. Data sources as in Fig. 12 caption.

the possible roles of lower and upper crust in their petrogenesis, an approach necessitated by the very large volumes of associated coeval silicic magmatism (see Part II), and the correlation between Sr isotopic compositions and increasing SiO_2 of the lavas (Fig. 16). We believe that the low-Ti basalt geochemistries can be explained

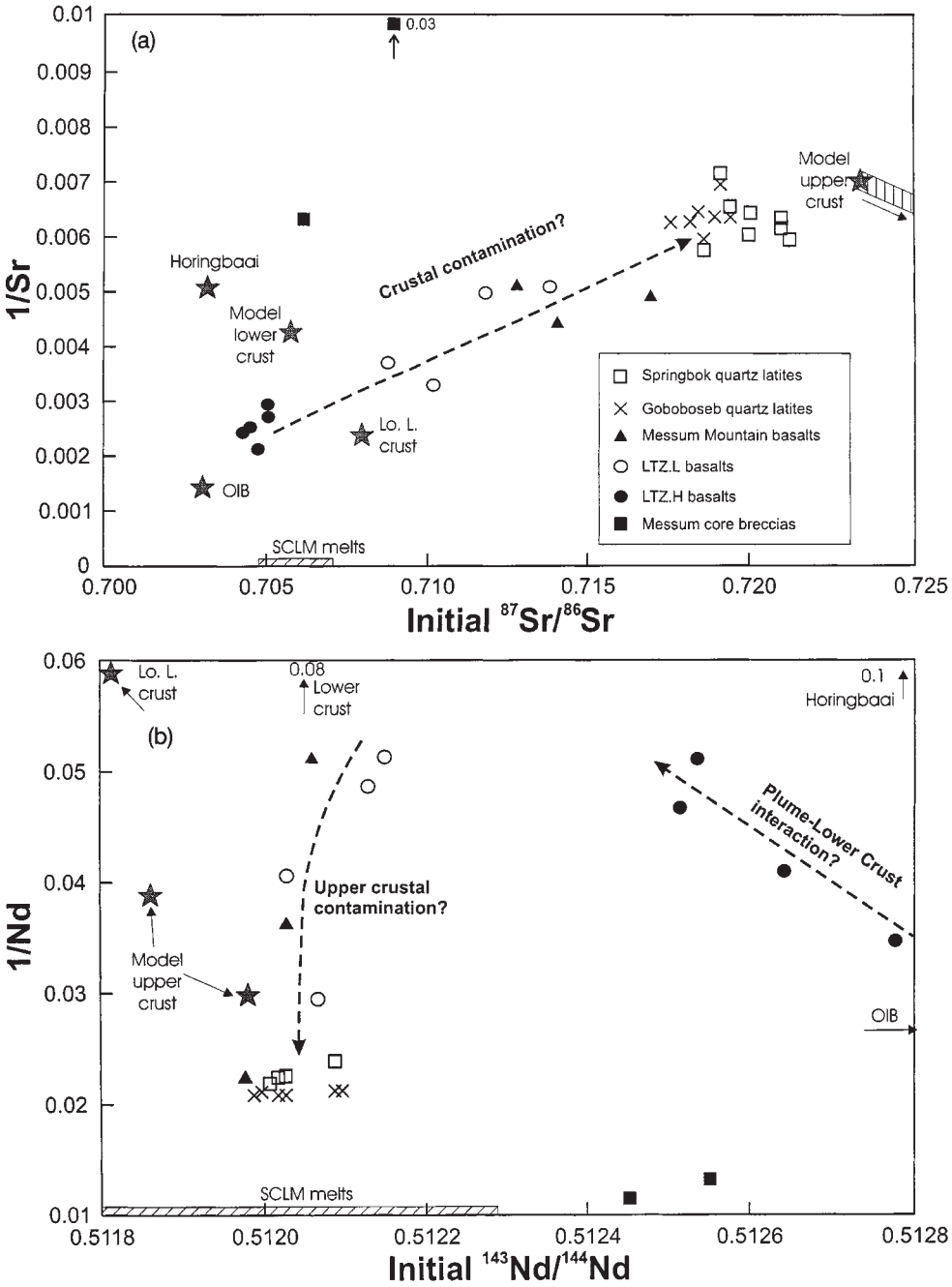

Fig. 15. $1/Sr–^{87}Sr/^{86}Sr$ (initial) and $1/Nd–^{143}Nd/^{144}Nd$ (initial) of the Goboboseb mafic and silicic eruptive phases, compared with various model crustal and SCLM end-member compositions, OIB, and the Horingbaai 'MORB-like' dolerites. Model compositions after Taylor & McLennan (1985), McDonough (1990), Rudnick & Presper (1990) and Gibson *et al.* (1995).

by major crustal input without a priori assumption of an SCLM source (e.g. Arndt & Christensen, 1992; Arndt *et al.*, 1993). A contribution from the SCLM cannot be uniquely excluded by our data, and comparisons are made between inferred SCLM compositions (Zartman & Haines, 1988; McDonough, 1990; Gibson *et al.*, 1995) and observed melt compositions.

End-member compositions

Possible scenarios are presented (Fig. 17), based on simple mixing of three end members: plume melt, mafic lower crust and silicic crust. The 'plume' end member is represented by LTZ.H sample SMG-127 (Appendix, Table A1), with the most Mg-rich and least evolved Sr and Nd isotopic compositions. Two model mafic lower-crustal

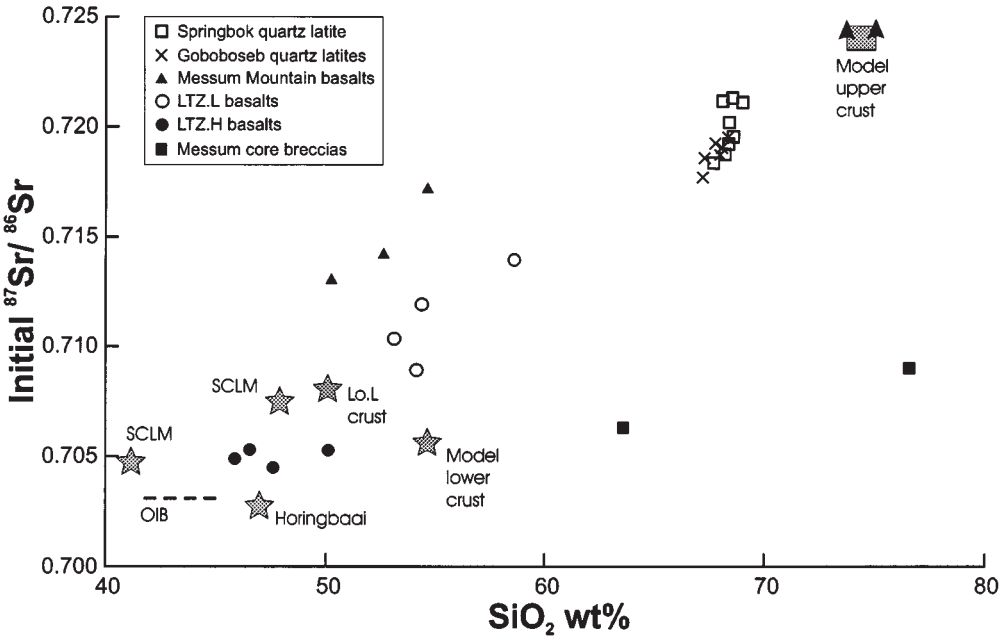

Fig. 16. Initial $^{87}Sr/^{86}Sr$–SiO_2 plot for the Goboboseb mafic and silicic phases, compared with various potential end-member compositions (data sources as in Fig. 15 caption).

compositions are used: the model composition of Taylor & McLennan [1985; with model isotopes from Zartman & Haines (1988)] and the mafic lowest lower-crustal (Lo.L. crust) xenolith average of Rudnick & Presper (1990). Isotopic compositions are selected from a compilation of mafic to intermediate basement Sr–Nd data from both Namibia and Namaqualand (the southern extension of the Namibian intercratonic mobile melt into South Africa), which show a rather wide range of isotopic compositions (ε_{Sr132} −14 to 1310, ε_{Nd132} +6 to −14; Clifford *et al.*, 1969, 1975, 1981, 1995; Downing & Coward, 1981; Haack *et al.*, 1982; Kroner, 1982; Cornell *et al.*, 1986; Haack & Gohn, 1988; Reid *et al.*, 1988; McDermott *et al.*, 1989; Ziegler & Stoessel, 1989; Hoal, 1990; Kukla, 1993). In terms of major element chemistry, the lower-crustal xenolith composition is similar to the mafic granulitic lower-crustal chemistries documented by Moore (1989; Appendix, Table A1), but these are not used because of the more complete data set available for the Rudnick & Presper (1990) average. The isotopic data suggest that Late Proterozoic crust (i.e. Damara equivalent), rather than an older silicic basement component, represents more plausible silicic crustal end members for the Awahab quartz latite magmas (see Part II). Two specific compositions are selected, both from the Damara equivalents in the Brazilian Parana Basin, namely the Pelotas Batholith (May, 1990; used because of the paucity of sufficiently complete chemical data from the Namibian basement). They comprise the earlier foliated granitoids (Cascata-type ~550–600 Ma) and the younger unfoliated granites (Cascata leucogranites, ~450–500 Ma; Appendix, Table A1).

RESULTS

Mixing fields (Fig. 17) calculated for combinations of the three end members suggest that, in terms of Sr–Nd space, the Goboboseb mafic (and silicic) volcanic compositions are broadly consistent with mixing between three end members, and with the exception of MMB, the silica contents of the lavas are also consistent (as shown by the calculated SiO_2 contours superimposed on the mixing fields in Fig. 17). Additional calculated curves shown in Fig. 17 are based on two separate 'mixed' mafic end-member starting compositions, representing 75:25 weight proportions of, first, the model lower crust and sample SMG-127, and, second, the Lo.L. crust and SMG-127, respectively (Appendix, Table A1). In these models, the isotopic compositions of the LTZ.L lavas (excepting the MMB), are more consistent with the younger Cascata-like silicic 'crustal' end member, than with the older, foliated granitic end-member compositions. Although the two estimates of the Sr and Nd isotopic compositions of the southern Brazilian SCLM (Gibson *et al.*, 1995) also lie close to the calculated 'lower crust–plume' mixing

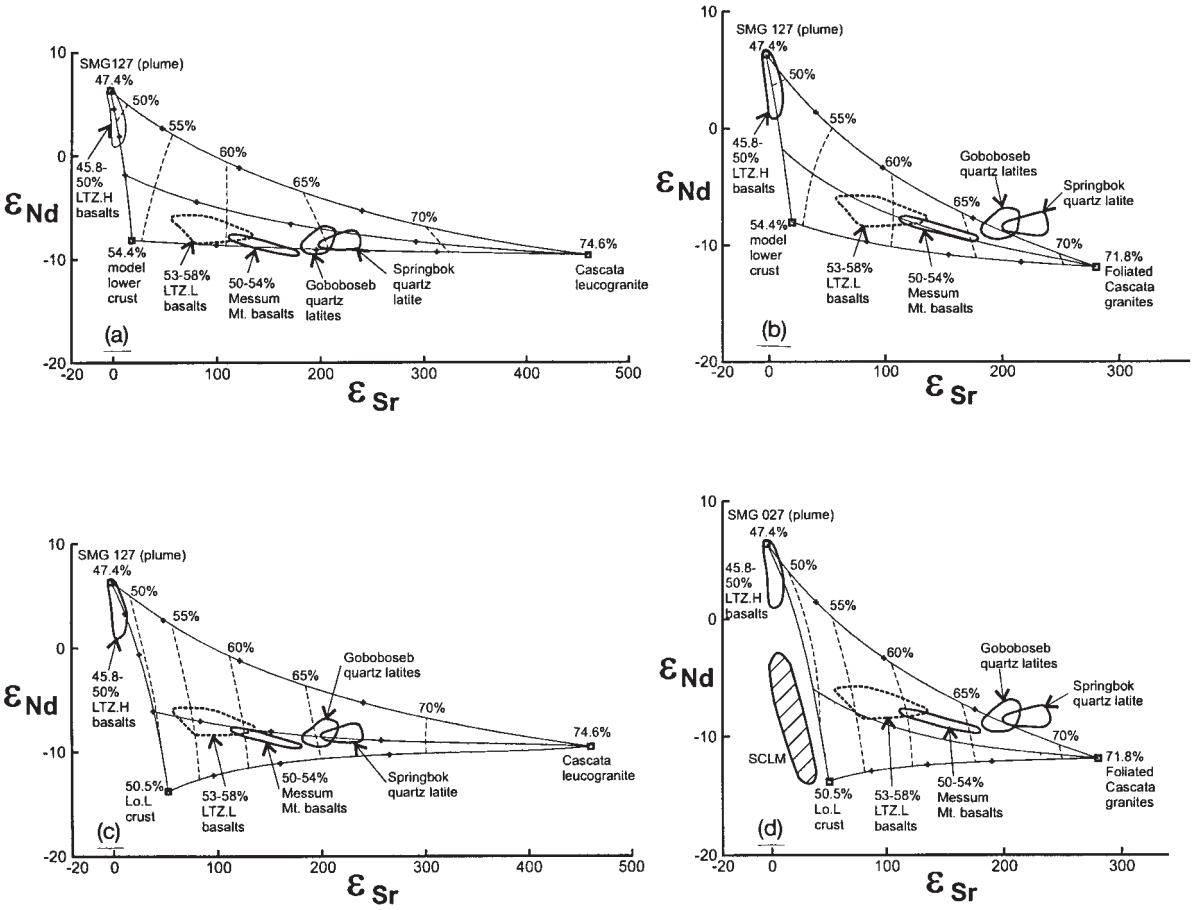

Fig. 17. ε_{Nd}–ε_{Sr} plots of four proposed scenarios involving crustal mixing between: (a) LTZ.H basalt (sample SMG127; equated with assumed 'plume' melt) plus model lower crust plus Cascata leucogranite; (b) SMG127 plus model lower crust plus foliated Cascata granite; (c) SMG127 plus model Lo.L. crust plus Cascata leucogranite; (d) SMG127 plus model Lo.L. crust plus foliated Cascata granites. The dotted curves are lines of equal % SiO_2. The heavy dots along the mixing curves represent 25% mixing intervals. Also shown are the generalized composition fields for the LTZ.H, LTZ.L and Messum Mountain basalts, and the Goboboseb and Springbok quartz latites, with the range of SiO_2 contents for all analysed samples within each of these groups shown. The SCLM (Gibson *et al.*, 1995) is also shown in (d), for comparison.

curves (Fig. 17), the Sr isotopic data require a more silicic crustal input to the LTZ and LTZ.L melts. Significantly, Martinez *et al.* (1996) and Milner & Le Roex (1996) showed that crustal contamination is supported by oxygen isotope data in the comparable tholeiitic series of the Okenyenya igneous complex. The Sr and Nd isotopic fields exhibited by the LTZ.H basalts (Fig. 17) are consistent with mixing between the assumed 'plume' and either of the mafic lower-crust end members, and/or the inferred Brazilian SCLM compositions.

As Fig. 17 is based only on Sr and Nd isotopic data, it is relevant to compare the modelled isotopic trends and end members with diagnostic trace element parameters. In Fig. 3, the Ti/Y and Ti/Zr ratios show good diagnostic trends between the various basaltic series. Ti/Y vs initial Sr and Nd isotopic ratios are therefore plotted (Fig. 18), with comparative regional Etendeka LTZ and HTZ basaltic compositions. The Sr (and Pb isotopic compositions, not shown) are negatively correlated with Ti/Y ratios, contrasting with Nd isotopic compositions which are positively correlated. Comparable Ti/Zr plots show similar patterns. In Fig. 18, the regional LTZ and LTZ.L basaltic fields again overlap, although the MMB series tend to be transitional towards the quartz latite compositions. To illustrate possible interrelationships, mixing curves are again plotted, linking the Cascata leucogranite end member with the model Lo.L. crust, the sample SMG127 ('plume') and the mixed Lo.L. crust + 'plume' end-member compositions (Appendix, Table A1). These curves are consistent with the

involvement of a silicic, crustal end member (again favouring the younger Cascata leucogranite-type composition relative to the foliated Cascata compositions), but further suggest the incorporation of mafic lower crust into the LTZ.L (and LTZ) basaltic melts, plus a variable 'plume' melt signature. The generalized Atlantic OIB and MORB fields shown (Fig. 18) further support the affinities of the LTZ.H melts with OIB-like melts, but show little evidence for MORB involvement in the LTZ.H or LTZ.L petrogenesis. In summary, the well-defined Ti/Y and Ti/Zr trends (Fig. 3) are isotopically correlated, and are suggested to be consistent with the generalized models presented in Fig. 17.

Modelling of specific LTZ.L mafic lava units

Messum Mountain Basalts

These represent (e.g. Fig. 6) a geochemically coherent sequence of lavas, varying from high-Mg basalts through to ferrobasalt. Bulk chemical changes are correlated with isotopic changes, with ε_{Sr} ranging from 116 to 175, and ε_{Nd} from –8·0 to –9·5, but with little change of Pb isotopes, implying AFC processes. Two general AFC models are suggested (Table 6), the first with cpx + ol + pl + mag + apatite phase assemblage and assimilation of Springbok quartz latite composition. Major element fits are good, as are most of the trace elements, including calculated Eu anomalies. The major problem is the low calculated ε_{Sr} (and to a less extent ε_{Nd}), a reflection of the small *r*-value (ratio of assimilation/crystallization) required by the least-squares fit. Similarly good major element fits are obtained with the two Cascata silicic end members used in this work, but again with the same calculated ε_{Sr} problem.

The second model uses a cpx + ol + pl phase assemblage and a composition from the Upper Damaran turbidite sediment of the Kuiseb Group (with ε_{Sr} and ε_{Nd} taken from the Kuiseb sediment average; see Part II). This provides good major element fits, acceptable trace element agreement (noting the lack of magnetite in the phase assemblage resulting in high calculated V), and importantly, because of the higher calculated *r*-value, gives much closer calculated isotopic compositions. Addition of magnetite to the phase assemblage, although still giving good least-squares fits and improving the V discrepancy, does result in lower *r*-value and thus poorer isotopic agreement.

The conclusion reached is that an AFC model is appropriate to explain the evolution of the MMB, but most plausibly involves an upper-crustal (i.e. younger) Damaran sediment end member, implying a relatively shallow magma system (3–4 km). Based on the tight geochemical coherence shown by the lavas, a single interconnected magma reservoir system is suggested.

Copper Valley icelandite

This homogeneous, voluminous, near-aphyric flow, with $\varepsilon_{Sr} = 130$ and $\varepsilon_{Nd} -7{\cdot}9$, again requires an AFC-type process to generate the relatively evolved Sr and Nd isotope signatures. All simple mixing models failed to give plausible results. The best fit AFC models utilize the most magnesian MMB (sample SMG-057) as parental composition. The three models presented (Table 7) illustrate the problems encountered in modelling this unit. The first model (cpx + pl + ol + Fe–Ti oxide phase assemblage) incorporates the Goboboseb QL (see Part II) as assimilant. This model provides reasonable major element fits (noting the K_2O and Na_2O discrepancies), and some notable trace element discrepancies (especially Ba and V, the latter because of the necessity to incorporate significant magnetite into this model). The model does, however, provide good isotopic fits, and reproduces observed Eu anomalies. The second model incorporates a Damaran Kuiseb turbidite composition, using the same phase assemblage. The results also show K_2O, Ba and V discrepancies, and result in isotopic compositions somewhat higher than the previous model. The third model incorporates the Cascata leucogranite, with the same phase assemblage. In this case, the Ba and K_2O discrepancies remain, but V shows good agreement (because of the magnetite required), but is definitely too high in calculated ε_{Sr} and ε_{Nd}. Similar problems are found for other silicic assimilant end members. Eu anomalies are again reproduced.

Attempts to model the Copper Valley flow are therefore only marginally satisfactory. On balance, it is believed that incorporation of the Goboboseb QL component into the parental basalt provides the most likely scenario (consistent with the stratigraphy of the units). One additional factor that lends support to the input of the Goboboseb QL magma, or its partly solidified products, into the liquid line of descent leading to the Copper Valley icelandite is that the inferred AFC processes would have occurred at high temperatures, not only favouring relatively high *r*-values, but facilitating the eruption of a relatively large volume, homogeneous, high-temperature (>1000°C) evolved icelandite.

SUMMARY

(1) The Goboboseb Mountains enclose a major bimodal eruptive centre within the southern Etendeka CFB Province which, based on the latest data, we believe were erupted in a very short interval at 132 Ma.

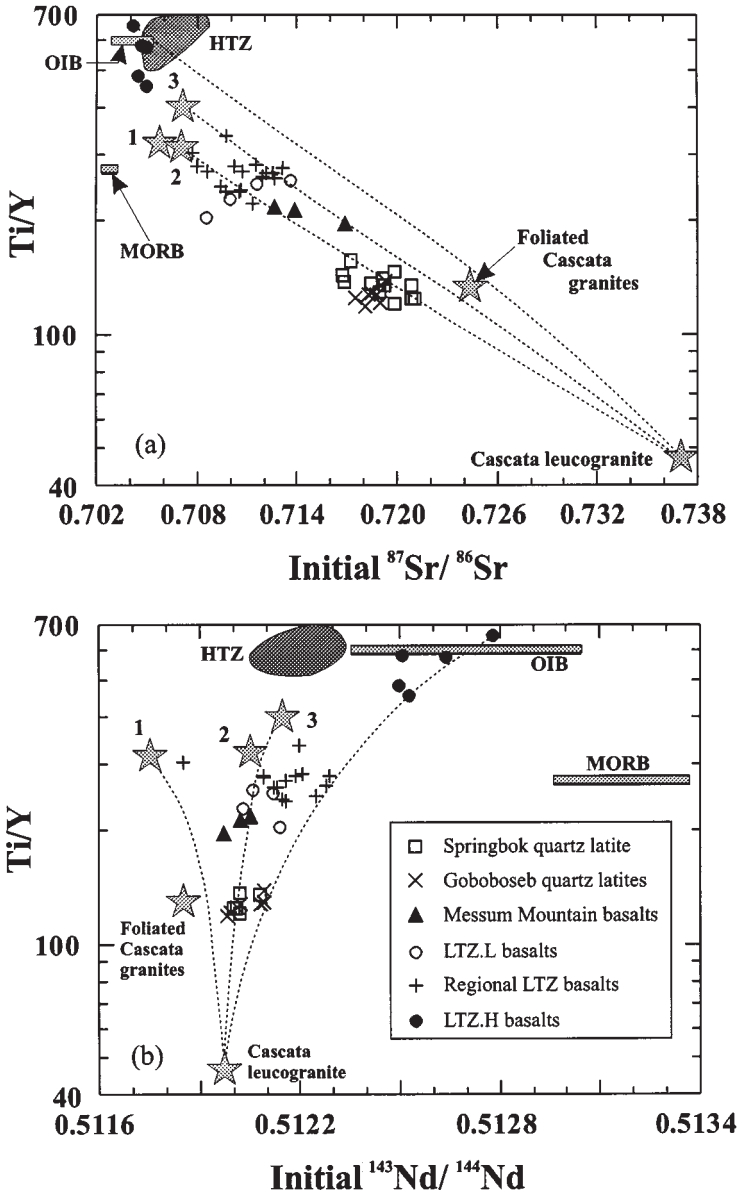

Fig. 18. Ti/Y ratios vs initial Sr and Nd isotopic compositions (at 132 Ma) for the Goboboseb volcanic series, and the regional Etendeka HTZ (field only) and LTZ basaltic series. The two upper-crustal and two lower-crustal (1, model lower crust; 2, Lo.L. crust) model compositions are shown, plus the mixed 'plume' + L.Lo. crust end-member composition (3) (see Fig. 17), together with generalized Atlantic MORB and central–southern Atlantic OIB compositions [after Sun & McDonough (1989) and sources listed in Fig. 12 caption). Three sets of mixing curves are shown, each linking to the Cascata leucogranite end member.

(2) The mafic lavas are shown to define two chemically, isotopically and mineralogically distinct series, named here as the LTZ.L and LTZ.H series. The LTZ.L series are tholeiitic and are characterized by relatively low MgO, and Ti/Zr, Sm/Yb and Ti/Y ratios; consistent Eu/Eu* negative anomalies; generally higher alkalis and radiogenic Pb isotopes; and evolved Sr and low Nd isotope compositions. They are equivalent to the Etendeka regional low Ti–Zr (LTZ or Tafelberg-type) basalts, and it is confirmed that they are closely similar to the Paraná Gramado basalt series. The LTZ.H series have no described extrusive equivalent within the Etendeka (or Parana), although Milner & le Roex (1996) have recently described isotopically similar alkaline gabbros from the Okenyenya igneous (subvolcanic) complex, some 100 km ENE of Messum. A sequence of basalts within Messum, the Messum Crater Basalts, are believed to represent an early volcanic phase in the overall Goboboseb sequence, and exhibit transitional chemistry between the LTZ.L and LTZ.H types.

Table 6: Least-squares AFC models linking least and most evolved Messum Mountain basalt lavas

Starting composition: SMG057 (high-Mg basalt)			
Target composition: SMG052 (ferrobasalt)			SMG057
assimilated material: Springbok QL[1]			SMG052
[1]Fractionating phases (wt %):			Damara Greywacke[1]
		Cpx 19·7	Cpx 15·87
		Oliv (Fo_{77}) 24·53	Oliv (Fo_{77}) 26·91
		Pl (An_{70}) 54·28	Pl (An_{77}) 57·22
		Magnetite 1·91	
		Apatite 0·11	
F-value		0·456	0·591
r-value		0·067	0·30
R^2		0·008	0·24
	Actual	Estimated[2]	Estimated[2]
SiO_2 (wt %)	54·44	54·43	54·41
TiO_2	1·81	1·87	1·98
Al_2O_3	14·90	14·90	14·97
FeO^+	11·85	11·83	11·86
MnO	0·20	0·25	0·22
MgO	4·06	4·07	4·07
CaO	7·35	7·35	7·39
Na_2O	2·47	2·48	2·04
K_2O	2·64	2·67	2·75
P_2O_5	0·28	0·27	0·31
Rb (ppm)	79·8	97	103
Ba	657	699	675
Sr	203	211	198
Zr	305	297	271
Nb	23·5	21	20
Cr	6·7	0·7	16
V	245	269	400
Sc	28	33	41
Ni	15	0·8	3·4
Pb	4·7	5·2	5·7
Zn	115	131	142
Cu	23	152	127
Y	56	58	55
La	43·7	36·5	33·2
Ce	91·1	78·9	73·7
Nd	44·7	40·7	39·8
Yb	5·18	5·7	4·3
Eu/Eu*	0·85	0·82	0·87
ε_{Sr}	174	120	169
ε_{Nd}	−9·4	−8·05	−8·4

[1]See Appendix, Table A1, for details of model compositions used.
[2]Basaltic partition coefficients used.

Table 7: Least-squares AFC models to test derivation of Copper Valley icelandic flow from least evolved MMB lava

Parent composition: SMG057 (high-Mg basalt)							
Assimilant:		Goboboseb QL		Damara greywacke[1]		Cascata leucogranite[1]	
Fractionating phases (wt %):		Cpx	14·97	Cpx	15·01	Cpx	13·18
		Oliv (Fo_{86})	25·43	Oliv (Fo_{85})	23·77	Pl (An_{75})	58·90
		Pl (An_{80})	56·14	Pl (An_{75})	56·60	Magnetite	0·64
		Magnetite	3·46	Magnetite	4·62	Oliv (Fo_{85})	27·28
Partition coefficient type:[2]		Basaltic	Andesitic	Basaltic	Andesitic	Basaltic	Andesitic
F-value		0·550		0·419		0·597	
r-value		0·21		0·109		0·26	
R^2		1·01		0·74		0·57	
	Actual	Estimated		Estimated		Estimated	
SiO_2 (wt %)	58·44	58·10		58·22		58·19	
TiO_2	1·71	1·46		1·38		1·62	
Al_2O_3	13·22	13·01		13·14		13·08	
FeO*	12·42	12·18		12·33		12·21	
MnO	0·17	0·26		0·22		0·23	
MgO	2·61	2·48		2·55		2·51	
CaO	6·26	6·24		6·29		6·22	
Na_2O	2·58	3·18		2·67		2·74	
K_2O	2·35	2·93		3·09		2·98	
P_2O_5	0·24	0·32		0·37		0·25	
Rb (ppm)	88·6	105	104	111	109	113	111
Ba	440	682	685	780	786	629	632
Sr	197	200	95	203	76	195	96
Zr	215	290	287	324	320	244	242
Nb	16	21	21	23	22	18	18
Cr	9·3	1·0	2·1	1·4	1·9	15	14
V	318	181	175	137	131	323	314
Sc	34	29	26	26	24	36	28
Ni	9·5	1·1	8·3	1·4	5·4	1·3	11
Pb	4·3	6·8	3·7	4·1	1·5	9·6	8·9
Zn	109	117	85	129	79	117	103
Cu	49·7	131	125	163	153	124	118
Y	40·3	57	58	66	66	50	50
La	32·8	37·0	37·0	39·0	39·0	32·4	32·4
Ce	70·1	80·5	80·5	85·9	85·9	68·5	68·5
Nd	34·3	41·2	41·2	45·7	45·7	35·4	35·4
Yb	3·8	5·4	5·4	5·8	5·8	4·6	4·6
Eu/Eu*	0·83	0·80	0·80	0·83	0·83	0·86	0·86
ε_{Sr}	130	123	126	142	159	160	180
ε_{Nd}	−7·86	−7·79	−7·79	−8·18	−8·18	−8·23	−8·23

[1]See Appendix, Table A1, for details of model compositions used.
[2]See Appendix, Table A2, for partition coefficients used.

(3) The LTZ.L series vary from high-Mg basalts to icelandites, with phenocryst assemblages of ± oliv + Pl + cpx ± Fe–Ti oxides, and groundmass pigeonitic and subcalcic pyroxenes. The LTZ.H series range from mildly alkaline (*ne*-normative) to tholeiitic, with phenocryst assemblages of oliv ± cpx in the more magnesian lavas, extending to cpx + pl ± oliv in the less magnesian samples. They fractionate to *ne*-benmoreite (phono-tephrite) magmas near the surface. The mineralogy is shown to correlate well with bulk whole-rock compositions, and relevant experimental phase boundaries, consistent with relatively low-pressure crystal fractionation processes.

(4) The LTZ.H melts are here identified as mantle plume dominated, specifically the Tristan da Cunha–Walvis Ridge plume. They show geochemical characteristics extending between E-MORB and OIB magmas. The differences, particularly in Ti/Y and Sm/Yb, between the LTZ.L and LTZ.H melts suggest that the latter show transitional signatures from melting in the garnet stability field (OIB-like) to the spinel peridotite field (MORB-like). The LTZ.H Pb–Nd–Sr isotopic compositions are similar to, but not identical with the modern Tristan compositions, and the observed variation in LTZ.H composition suggests limited mixing with an Atlantic MORB component, and/or lower crust and SCLM.

(5) The LTZ.L melts are more enigmatic, especially their geochemical 'arc signatures'. They exhibit, for example, correlated initial ε_{Sr} with SiO_2, Ti/Y, Ti/Zr and 1/Sr, and ε_{Nd} − 1/Nd, consistent with mixing–AFC processes involving both lower-crustal and upper silicic crustal input. These melts are modelled by three-component mixing (although AFC is a more plausible process), involving plume melt, mafic lower crust and silicic upper crust (the last using Damara equivalents from the Parana). The results support the plausibility of the LTZ.L melts as representing the products of such plume–crustal interactions, with the silicic quartz latite melts (see Part II) extending the trends and representing maximum silicic upper-crustal input. Nevertheless, the data cannot uniquely exclude SCLM input.

ACKNOWLEDGEMENTS

The authors all wish to remember and acknowledge the late Tony Erlank, who provided so much impetus and enthusiasm for research in the Etendeka. We are pleased to acknowledge extensive logistic support from the Geological Survey of Namibia, and financial support from the FRD, South Africa. Acknowledgement is made to M. Wilson, S. Turner and an anonymous reviewer for valuable input into drafts of this manuscript.

REFERENCES

Arndt, N. T. & Christiansen, U. (1992). The role of lithospheric mantle in continental flood volcanism: thermal and geochemical constraints. *Journal of Geophysical Research* **97**(B7), 10967–10981.

Arndt, N. T., Czamanske, G. K., Wooden, J. L. & Fedorenko, V. A. (1993). Mantle and crustal contributions to continental flood volcanism. *Tectonophysics* **223,** 39–52.

Baksi, A. K., Fodor, R. V. & Farrar, E. (1991). Preliminary results of $^{40}Ar/^{39}Ar$ dating studies on rocks from the Serra Geral flood basalt province and the Brazilian continental margin (Abstract). *EOS Transactions, American Geophysical Union* **72,** 300.

Bence, A. E. & Albee, A. L. (1968). Empirical correction factors for the electron microanalysis of silicates and oxides. *Journal of Geology* **76,** 382–403.

Carmichael, I. S. E. (1964). The petrology of Thingmuli, a Tertiary volcano in eastern Iceland. *Journal of Petrology* **5,** 435–460.

Chappell, B. W. & Hergt, J. M. (1989). The use of known Fe content as a flux monitor in neutron activation analysis. *Chemical Geology* **78,** 151–158.

Clifford, T. N., Rooke, J. M. & Allsopp, H. L. (1969). Petrochemistry and age of the Franzfontein granitic rocks of northern south-west Africa. *Geochimica et Cosmochimica Acta* **33,** 973–986.

Clifford, T. N., Gronow, J., Rex, D. C. & Burger, A. J. (1975). Geochronological petrogenetic studies of high-grade metamorphic rocks and intrusives in Namaqualand, South Africa. *Journal of Petrology* **16,** 154–188.

Clifford, T. N., Stumpfl, E. F., Burger, A. J., McCarthy, T. S. & Rex, D. C. (1981). Mineral-chemical and isotopic studies of Namaqualand granulites, South Africa: a Grenville analogue. *Contributions to Mineralogy and Petrology* **77,** 225–250.

Clifford, T. N., Barton, E. S., Retief, E. A., Rex, D. C. & Fanning, C. M. (1995). A crustal progenitor for the intrusive anorthosite–charnockite kindred of the cupriferous Koperberg suite O'okiep District, Namaqualand, South Africa; new isotope data for the country rocks and the intrusives. *Journal of Petrology* **36,** 231–258.

Cohen, R. S. & O'Nions, R. K. (1982). The lead, neodymium and strontium isotopic structure of ocean ridge basalts. *Journal of Petrology* **23,** 299–324.

Cohen, R. S., Evensen, N. M., Hamilton, P. J. & O'Nions, R. K. (1980). U–Pb, Sm–Nd and Rb–Sr systematics of mid-ocean ridge basalt glasses. *Nature* **283,** 149–153.

Cornell, D. H., Hawkesworth, C. J., van Calsteren, P. & Scott, W. D. (1986). Sm–Nd study of Precambrian crustal development in the Prieska–Copperton region, Cape Province. *Transactions of the Geological Society of South Africa* **89,** 17–28.

Cox, K. G. (1993). Continental magmatic underplating. *Philosophical Transactions of the Royal Society of London, Series A* **342,** 155–166.

Cox, K. G., Duncan, A. R., Bristow, J. W., Taylor, S. R. & Erlank, A. J. (1984). Petrogenesis of the basic rocks of the Lebombo. In: Erlank, A. J. (ed.) *Geological Society of South Africa, Special Publication* **13,** 149–170.

Downing, K. N. & Coward, M. P. (1981). The Okahandja lineament and its significance for Damaran tectonics in Namibia. *Geologische Rundschau* **70,** 972–1000.

Duncan, A. R. (1987). The Karoo Igneous Province—a problem area for inferring tectonic setting from basalt geochemistry. *Journal of Volcanogy and Geothermal Research* **32,** 13–34.

Duncan, A. R., Newton, S. R., van den Berg, C. & Reid, D. L. (1989). Geochemistry and petrology of dolerite sills in the Huab River Valley, Damaraland, north-western Namibia. *Communications of the Geological Survey of Namibia* **5,** 5–17.

Duncan, A. R., Armstrong, R. A., Erlank, A. J., Marsh, J. S. & Watkins, R. T. (1990). MORB-related dolerites associated with the final phase of Karoo flood basalt volcanism in Southern Africa. In: Parker, A. J., Rickwood, P. C. & Hunter, D. H. (eds) *Mafic Dykes and Emplacement Mechanisms. Proceedings of 2nd International Dyke Conference*. Rotterdam: A. A. Balkema, pp. 119–130.

Dupre, B. & Allegre, C. J. (1980). Pb–Sr–Nd isotopic correlation and the chemistry of the North Atlantic mantle. *Nature* **286,** 17–22.

Erlank, A. J., Marsh, J. S., Duncan, A. R., Miller, R. McG., Hawkesworth, C. J., Betton, P. J. & Rex, D. C. (1984). Geochemistry and petrogenesis of the Etendeka volcanic rocks from SWA/Namibia. In: Erlank, A. J. (ed.) *Geological Society of South Africa, Special Publication* **13,** 195–245.

Ewart, A., Bryan, W. B., Chappell, B. W. & Rudnick, R. L. (1994). Regional geochemistry of the Lau–Tonga arc and backarc systems. In: Hawkins, J., Parson, L., Allan, J., *et al.* (eds) *Proceedings of the Ocean Drilling Program, Scientific Results, 135*. College Station, TX: Ocean Drilling Program, pp. 385–425.

Ewart, A., Milner, S. C., Armstrong, R. A. & Duncan, A. R. (1998). Etendeka volcanism of the Goboboseb Mountains and Messum Igneous Complex, Namibia. Part II: Voluminous quartz latite volcanism of the Awahab magma system. *Journal of Petrology* **39,** 227–253

Farnetani, C. G., Richards, M. A. & Ghiorso, M. S. (1996). Petrological models of magma evolution and deep crustal structure beneath hot spots and flood basalt provinces. *Earth and Planetary Science Letters* **143,** 81–94.

Fitton, J. G., James, D. & Leeman, W. P. (1991). Basic magmatism associated with late Cenozoic extension in the western United States: compositional variations in space and time. *Journal of Geophysical Research* **96**(B8), 13693–13711.

Garland, F., Hawkesworth, C. J. & Mantovani, M. S. M. (1995). Description, and petrogenesis of the Parana rhyolites, southern Brazil. *Journal of Petrology* **36,** 1193–1227.

Gibson, S. A., Thompson, R. N., Dicken, A. P. & Leonardos, O. H. (1995). High-Ti and Low-Ti mafic potassic magmas: key to plume–lithosphere interactions and continental flood-basalt genesis. *Earth and Planetary Science Letters* **136,** 149–165.

Haack, U. & Gohn, E. (1988). Rb–Sr data on some pegmatites in the Damara orogen (Namibia). *Communications of the Geological Survey of South West Africa/Namibia* **4,** 13–17.

Haack, U., Hoefs, J. & Gohn, E. (1982). Constraints on the origin of Damaran granites by Rb/Sr and $\delta^{18}O$ data. *Contributions to Mineralogy and Petrology* **79,** 279–289.

Harris, C., Bell, J. D. & Atkins, F. B. (1982). Isotopic composition of lead and strontium in lavas and coarse grained blocks from Ascension Island, South Atlantic. *Earth and Planetary Science Letters* **60,** 79–85.

Hawkesworth, C. J., Marsh, J. S., Duncan, A. R., Erlank, A. J & Norry, M. J. (1984). The role of continental lithosphere in the generation of the Karoo volcanic rocks: evidence from combined Nd- and Sr-isotope studies. In: Erlank, A. J. (ed.) *Geological Society of South Africa, Special Publication* **13,** 341–354.

Hawkesworth, C. J., Gallagher, K., Kelley, M., Mantovani, M., Peate, D. W., Regelous, M. & Rogers, N. W. (1992). Parana magmatism and the opening of the South Atlantic. In: Story, B. C., Alabaster, T. & Pankhurst, R. J. (eds) *Magmatism and the Causes of Continental Break-up. Geological Society, London, Special Publication* **68,** 221–240.

Henry, G., Clendenin, C. W., Stanistreet, I. G. & Maiden, K. J. (1990). Multiple detachment model for the early rifting stage of the Late Proterozoic Damara orogen in Namibia. *Geology* **18,** 67–71.

Hergt, J. M., Peate, D. W. & Hawkesworth, C. J. (1991). The petrogenesis of Mesozoic Gondwana low-Ti flood basalts. *Earth and Planetary Science Letters* **105,** 134–148.

Hoal, B. G. (1990). The geology and geochemistry of the Proterozoic Awasib Mountain Terrain, Southern Namibia. *Geological Survey of Namibia Memoir* **11,** 163 pp.

Korn, H. & Martin, H. (1954). The Messum igneous complex in Southwest Africa. *Transactions of the Geological Society of South Africa* **57,** 83–124.

Kroner, A. (1982). Rb–Sr geochronology and tectonic evolution of the pan-African Damara belt of Namibia, Southwestern Africa. *American Journal of Science* **282,** 1471–1507.

Kukla, C. (1993). Strontium isotope heterogeneities in amphibolite facies, banded metasediments. A case study from the Late Proterozoic Kuiseb Formation of the Southern Damara orogen, Central Namibia. *Geological Survey of Namibia Memoir* **15,** 139 pp.

le Roex, A. P. (1985). Geochemistry, mineralogy and magmatic evolution of the basaltic and trachytic lavas from Gough Island, South Atlantic. *Journal of Petrology* **26,** 149–186.

le Roex, A. P., Cliff, R. A. & Adair, B. J. I. (1990). Tristan da Cunha, South Atlantic: geochemistry and petrogenesis of a basanite–phonolite lava series. *Journal of Petrology* **31,** 779–812.

Lindsley, D. H. (1983). Pyroxene thermometry. *American Mineralogist* **68,** 477–493.

Martin, H., Mathias, M. & Simpson, E. S. W. (1960). The Damaraland sub-volcanic ring complexes in south west Africa. In: Sorgenfrei, T. (ed.) *Report of the International Geological Congress XXI Session 13*. Copenhagen: Norden, pp. 156–174.

Martinez, I. A., Harris, C., le Roex, A. P. & Milner, S. C. (1996). Oxygen isotope evidence for extensive crustal contamination in the Okenyenya igneous complex, Namibia. *Geochimica et Cosmochimica Acta* **60,** 4497–4508.

May, S. E. (1990). Pan-African magmatism and regional tectonics of South Brazil. Ph.D. Thesis, The Open University, Milton Keynes, UK, 343 pp.

McDermott, F., Harris, N. B. W. & Hawkesworth, C. J. (1989). Crustal reworking in southern Africa: constraints from Sr–Nd isotope studies in Archaean to Pan-African terrains. *Tectonophysics* **161,** 257–270.

McDonough, W. F. (1990). Constraints on the composition of the continental lithospheric mantle. *Earth and Planetary Science Letters* **101,** 1–18.

Miller, R. McG. (1983). The Pan-African Damara orogen of south west Africa/Namibia. In: Miller, R. McG. (ed.) *Geological Society of South Africa, Special Publication* **11,** 431–515.

Milner, S. C. & Ewart, A. (1989). The geology of the Goboboseb Mountain volcanics and their relationship to the Messum Complex, Namibia. *Communications of the Geological Survey of Namibia* **5,** 31–40.

Milner, S. C. & le Roex, A. P. (1996). Isotope characteristics of the Okenyenya igneous complex, northwestern Namibia: constraints on the composition of the early Tristan plume and the origin of the EM1 mantle component. *Earth and Planetary Science Letters* **141,** 277–291.

Milner, S. C., Duncan, A. R. & Ewart, A. (1992). Quartz latite rheoignimbrite flows of the Etendeka Formation, north-western Namibia. *Bulletin of Volcanology* **54,** 200–219.

Milner, S. C., Duncan, A. R., Ewart, A. & Marsh, J. S. (1995*a*). Promotion of the Etendeka Formation to Group status: a new integrated stratigraphy. *Communications of the Geological Survey of Namibia* **9,** 5–11.

Milner, S. C., Duncan, A. R., Whittingham, A. M. & Ewart, A. (1995*b*). Trans-Atlantic correlation of eruptive sequences and individual silicic volcanic units within the Parana–Etendeka igneous province. *Journal of Volcanology and Geothermal Research* **69,** 137–157.

Milner, S. C., le Roex, A. P. & O'Connor, J. M. (1995*c*). Age of Mesozoic igneous rocks in northwestern Namibia, and their

relationship to continental breakup. *Journal of the Geological Society, London* **152,** 97–104.

Moore, J. M. (1989). A comparative study of metamorphosed supracrustal rocks from the western Namaqualand metamorphic complex. *Chamber of Mines Precambrian Research Unit, Bulletin 37*. Department of Geology, University of Cape Town, 370 pp.

Norrish, K. & Hutton, J. T. (1969). An accurate X-ray spectrographic method for the analysis of a wide range of geological samples. *Geochimica et Cosmochimica Acta* **32,** 431–453.

O'Connor, J. M. & Duncan, A. R. (1990). Evolution of the Walvis Ridge and Rio Grande Rise hotspot system—implications for African and South American plate motions over plumes. *Journal of Geophysical Research* **95,** 17475–17502.

O'Connor, J. M. & le Roex, A. P. (1992). South Atlantic hotspot–plume systems. I. Distribution of volcanism in time and space. *Earth and Planetary Science Letters* **113,** 343–364.

O'Nions, R. K. & Pankhurst, R. J. (1974). Petrogenetic significance of isotope and trace element variations in volcanic rocks from the Mid Atlantic. *Journal of Petrology* **15,** 603–634.

O'Nions, R. K., Hamilton, P. J. & Evensen, N. M. (1977). Variations in $^{143}Nd/^{144}Nd$ and $^{87}Sr/^{86}Sr$ ratios in oceanic basalts. *Earth and Planetary Science Letters* **34,** 13–22.

Peate, D. W. (1989). Stratigraphy and petrogenesis of the Paraná continental flood basalts, Southern Brazil. Ph.D. Thesis, Open University, Milton Keynes, UK, 359 pp.

Peate, D. W. & Hawkesworth, C. J. (1996). Lithospheric to asthenospheric transition in low-Ti flood basalts from southern Parana, Brazil. *Chemical Geology* **127,** 1–24.

Peate, D. W., Hawkesworth, C. J., Mantovani, M. S. M. & Shukowsky, W. (1990). Mantle plumes and flood-basalt stratigraphy in the Parana, South America. *Geology* **18,** 1223–1226.

Peate, D. W., Hawkesworth, C. J. & Mantovani, M. S. M. (1992). Chemical stratigraphy of the Parana lavas (South America): classification of magma types and their spatial distribution. *Bulletin of Volcanology* **55,** 119–139.

Reid, D. L., Malling, S. & Allsopp, H. L. (1988). Rb-Sr ages of granitoids in the Rehoboth Nauchas area, southwest Africa/Namibia. *Communications of the Geological Survey of Southwest Africa/Namibia* **4,** 19–27.

Renne, P. R., Ernesto, M., Pacca, I. G., Coe, R. S., Glen, J. M., Prevot, M. & Perrin, M. (1992). The age of Parana flood volcanism, rifting of Gondwanaland, and the Jurassic–Cretaceous boundary. *Science* **258,** 975–979.

Renne, P. R., Deckart, K., Ernesto, M., Feraud, G. & Piccirillo, E. M. (1996*a*). Age of the Ponta Grossa dike swarm (Brazil), and implications to Parana flood volcanism. *Earth and Planetary Science Letters* **144,** 199–211.

Renne, P. R., Glen, J. M., Milner, S. C. & Duncan, A. R. (1996*b*). Age of Etendeka flood volcanism and associated intrusions in southwestern Africa. *Geology* **24,** 659–662.

Richardson, S. H., Erlank, A. J., Duncan, A. R. & Reid, D. L. (1982). Correlated Nd, Sr and Pb isotope variation in Walvis Ridge basalts and implications for the evolution of their mantle source. *Earth and Planetary Science Letters* **59,** 327–342.

Richardson, S. H., Erlank, A. J., Reid, D. L. & Duncan, A. R. (1984). Major and trace elements and Nd and Sr isotope geochemistry of basalts from the Deep Sea Drilling Project leg 74 Walvis Ridge transect. *Initial Reports of the Deep Sea Drilling Project, 74*. Washington, DC: US Government Printing Office, pp. 739–754.

Rudnick, R. L. & Presper, T. (1990). Geochemistry of intermediate- to high-pressure granulites. In: Vielzeuf, D. & Vidal, Ph. (eds) *Granulites and Crustal Evolution*. Dordrecht: Kluwer Academic, pp. 523–550.

Stewart, K., Turner, S., Kelley, S., Hawkesworth, C., Kirsten, L. & Mantovani, M. (1996). 3-D, ^{40}Ar–^{39}Ar geochronology in the Parana continental flood basalt province. *Earth and Planetary Science Letters* **143,** 95–109.

Sun, S.-S. & McDonough, W. F. (1989). Chemical and isotopic systematics of oceanic basalts: implications for mantle composition and processes. In: Saunders A. D. & Norry, M. J. (eds) *Magmatism in the Ocean Basins*. *Geological Society, London, Special Publication* **42,** 313–345.

Taylor, S. R. & McLennan, S. M. (1985). *The Continental Crust: its Composition and Evolution*. Cambridge, MA: Blackwell Scientific, 312 pp.

Turner, S., Regelous, M., Kelley, S., Hawkesworth, C. & Mantovani, M. (1994). Magmatism and continental break-up in the South Atlantic: high precision ^{40}Ar–^{39}Ar geochronology. *Earth and Planetary Science Letters* **121,** 333–348.

Walker, D., Shibata, T. & De Long, S. E. (1979). Abyssal tholeiites from the Oceanographer Fracture Zone. II. Phase equilibria and mixing. *Contributions to Mineralogy and Petrology* **70,** 111–125.

Watkins, R. T., McDougall, I. & Le Roex, A. P. (1994). K–Ar ages of the Brandberg and Okenyenya igneous complexes, north-western Namibia. *Geologische Rundshau* **83,** 348–356.

Weis, D. (1983). Pb isotopes in Ascension Island rocks: oceanic origin for the gabbroic to granitic plutonic xenoliths. *Earth and Planetary Science Letters* **62,** 273–282.

White, R. & McKenzie, D. (1989). Magmatism at rift zones: the generation of volcanic continental margins and flood basalts. *Journal of Geophysical Research* **94**(B6), 7685–7729.

Wood, D. A. (1978). Major and trace element variations in the Tertiary lavas of eastern Iceland and their significance with respect to the Iceland geochemical anomaly. *Journal of Petrology* **19,** 393–436.

Zartman, R. E. & Haines, S. M. (1988). The plumbotectonic model for Pb isotopic systematics among major terrestrial reservoirs—a case for bi-directional transport. *Geochimica et Cosmochimica Acta* **52,** 1327–1339.

Ziegler, U. R. F. & Stoessel, G. F. U. (1989). Report: K–Ar, Rb–Sr and geochemical investigations in the Mooirivier Complex, southwestern Windhoek District and north-western Maltahohe District, Namibia. *Communications of the Geological Survey of Namibia* **5,** 69–75.

APPENDIX

Table A1: Model compositions used in calculations

	SMG127 ('plume')	Lowest Lower crust[1] (Lo.L. crust)	Model Lower crust[2]	Namaqualand mafic granulites[3]	Foliated Cascata granitoids[4]	Cascata leucogranite[4]	Damara greywacke	Mixed 'plume' + Lo.L. crust (1:3 ratio)
SiO_2	47·44	50·50	54·40	50·13	71·80	74·62	59·67	49·73
TiO_2	2·31	1·04	1·00	1·48	0·45	0·18	0·84	1·36
Al_2O_3	10·27	16·50	16·10	17·15	14·38	13·66	17·18	14·94
FeO*	13·20	9·03	10·60	11·35	2·67	1·43	6·86	10·07
MnO	0·20	0·15	0·21	0·21	0·05	0·05	0·12	0·16
MgO	14·44	7·68	6·30	6·91	0·81	0·25	4·70	9·37
CaO	8·75	9·77	8·50	10·39	1·99	1·20	5·57	9·51
Na_2O	2·25	2·39	2·80	1·51	3·26	3·43	1·45	2·35
K_2O	0·90	0·79	0·34	0·66	4·47	5·10	3·36	0·82
P_2O_5	0·26	0·23	0·10	0·21	0·12	0·07	0·24	0·24
Rb	28·1	17	5·3	28	145	215	135	19·8
Ba	236	521	150	161	959	569	608	450
Sr	416	422	230	377	236	153	154	420
Zr	163	89	70	126	196	133	195	108
Nb	17·4	11	6·0	6	13·5	14	15·2	12·5
Cr	1160	308	235	200	25·0	18	115	521
V	368	214	285	251	48·0	25	177	253
Sc	23	34	36	41	7·0	2	22·2	31·2
Ni	670	137	135	94	6·5	3	67·8	270
Pb	2·6	5·0	4·0	10	23	30	10	4·4
Zn	100	90	83	101	59	41	136	92·5
Cu	168	53	90	14	13·4	8	22·8	81·7
Y	21·2	20	19	32	20	23	40	20·3
La	23·2	13·0	11·0	15	59·7	28·6	25·6	15·6
Ce	55·4	27·8	23·0	29	85·5	53·2	61·1	34·7
Nd	28·9	15·2	12·7	22	32·8	25·5	36·5	18·6
Yb	1·7	1·9	2·2	1·9	0·88	1·41	—	1·84
ε_{Sr}	−5·28	50·0	18·0	50·0	280	460	450	36·3
ε_{Nd}	6·21	−14·0	−8·3	−14	−12·0	−9·6	−9·68	−6·16

[1]Rudnick & Presper (1990). [2]Taylor & McLennan (1985), with isotopes from Zartman & Haines (1988). [3]Moore (1989). [4]May (1990).
$\delta^{18}O$ values assumed for SMG127, Lo.L. crust, Namaqualand mafic granulites and Cascata leucogranite are 5·50, 6·50, 6·50, and 12·0‰, respectively.

Table A2: Basaltic, andesitic, dacitic and quartz latite partition coefficients used in modelling calculations

	Basaltic					Dacitic				
	Plagioclase	Olivine	Augite	Orthopyroxene	Magnetite	Plagioclase	Olivine	Augite	Orthopyroxene	Magnetite
Rb	0·10	0·0002	0·011	0·0006	0·0040	0·08	0·0002	0·09	0·02	0·004
Ba	0·15	0·0086	0·077	0·014	0·40	0·20	0·0086	0·15	0·04	0·11
Sr	1·60	0·0002	0·10	0·07	0·10	4·4	0·0002	0·07	0·03	0·03
Zr	0·02	0·10	0·10	0·08	0·40	0·10	0·10	0·20	0·08	0·20
Nb	0·01	0·05	0·05	0·02	1·0	0·05	0·01	0·04	0·02	2·5
Cr	0·027	2·4	32·0	13·0	100	0·05	2·4	50·0	25·0	60·0
V	0·017	0·06	1·4	0·50	30·0	0·02	0·06	5·2	2·1	60·0
Sc	0·014	0·18	2·8	1·7	15·0	0·02	0·18	13·2	4·7	3·4
Ni	0·05	30·0	2·8	6·5	5·0	0·21	18·0	6·0	20·0	13·0
Pb	0·36	0·01	0·01	0·0013	0·30	0·58	0·10	0·10	0·10	0·30
Zn	0·10	1·2	0·50	1·2	5·4	0·15	1·2	2·3	4·0	18·0
Cu	0·10	0·06	0·50	0·10	1·0	0·25	0·05	0·5	0·10	1·0
Y	0·02	0·068	0·80	0·25	0·50	0·08	0·068	2·5	0·50	0·80
La	0·22	0·0018	0·16	0·24	0·45	0·25	0·0018	0·35	0·90	0·50
Ce	0·17	0·0018	0·22	0·30	0·42	0·20	0·0018	0·52	0·50	0·60
Nd	0·11	0·0018	0·36	0·14	0·44	0·20	0·0018	1·2	0·22	0·80
Yb	0·021	0·0094	0·56	0·26	0·47	0·04	0·0094	1·8	0·85	0·60

	Andesitic						Quartz latite			
	Plagioclase	Olivine	Augite	Orthopyroxene	Magnetite	Apatite	Plagioclase	Pigeonite	Magnetite	Apatite
Rb	0·14	0·0002	0·013	0·015	0·004	0·001	0·008	0·005	0·004	0·01
Ba	0·15	0·0086	0·024	0·014	0·40	0·014	0·72	0·083	0·10	0·014
Sr	3·5	0·0002	0·067	0·03	0·10	0·88	8·4	0·01	0·11	10·0
Zr	0·10	0·06	0·20	0·10	0·4	0·034	0·039	0·068	0·92	0·034
Nb	0·09	0·05	0·043	0·02	1·0	0·011	0·05	0·08	4·0	0·011
Cr	0·027	2·4	35·0	15·0	58·0	0·0	0·10	20·0	50·0	0·01
V	0·017	0·06	1·7	0·60	30·0	0·06	0·02	4·0	25·0	0·06
Sc	0·014	0·18	6·0	2·0	5·9	0·22	0·05	14·0	6·6	0·22
Ni	0·12	18·0	3·7	9·5	10·0	0·0	0·05	5·6	0·10	0·001
Pb	0·58	0·10	0·10	0·10	0·30	0·0	0·30	0·05	5·2	0·10
Zn	0·13	1·2	1·4	2·6	14·0	0·0	0·36	5·5	20·2	3·5
Cu	0·17	0·05	0·67	0·12	1·0	0·28	0·05	0·38	0·30	0·28
Y	0·04	0·09	2·4	0·46	0·5	2·5	0·04	1·2	0·86	70·0
La	0·22	0·0018	0·16	0·24	0·45	9·3	0·29	0·63	0·67	25·6
Ce	0·17	0·0018	0·22	0·30	0·42	9·6	0·24	0·78	0·75	33·4
Nd	0·11	0·0018	0·36	0·14	0·44	10·0	0·17	1·0	1·2	55·8
Yb	0·021	0·0094	0·56	0·26	0·47	6·45	0·042	1·6	0·60	64·7